LBL-8589

MASTER

COLLISIONS OF HALOGEN (^2P) AND RARE GAS (^1S) ATOMS

Christopher Hank Becker
(Ph. D. thesis)

December 1978

Prepared for the U. S. Department of Energy
under Contract W-7405-ENG-48

DISTRIBUTION OF THIS DOCUMENT IS UNLIMITED

LBL-8589

COLLISIONS OF HALOGEN (^2P) AND RARE GAS (^1S) ATOMS

Christopher Hank Becker

Materials and Molecular Research Division
Lawrence Berkeley Laboratory

and

Department of Chemistry
University of California
Berkeley, California 94720

December 1978

NOTICE

This report was prepared as an account of work sponsored by the United States Government. Neither the United States nor the United States Department of Energy, nor any of their employees, nor any of their contractors, subcontractors, or their employees, makes any warranty, express or implied, or assumes any legal liability or responsibility for the accuracy, completeness or usefulness of any information, apparatus, product or process disclosed, or represents that its use would not infringe privately owned rights.

ABSTRACT

Differential cross sections I(Θ) at several collision energies measured in crossed molecular beam experiments are reported for several combinations of halogen atoms (^2P) scattered off rare gas atoms ($^1S_0$), namely, F + Ne, F + Ar, F + Kr, F + Xe, and Cl + Xe. The scattering is described by an elastic model appropriate to Hund's case c coupling. With the use of this model, the $X\frac{1}{2}$, $I\frac{3}{2}$, and $II\frac{1}{2}$ interaction potential energy curves are derived by fitting calculated differential cross sections, based on analytic representations of the potentials, to the data. The F - Xe $X\frac{1}{2}$ potential shows a significant bonding qualitatively different than for the other F-rare gases. The $I\frac{3}{2}$ and $II\frac{1}{2}$ potentials closely resemble the van der Waals interactions of the one electron richer ground state rare gas-rare gas systems. Coupled-channel scattering calculations are carried out for F + Ar, F + Xe, and Cl + Xe using the realistic potential curves derived earlier. The results

DISTRIBUTION OF THIS DOCUMENT IS UNLIMITED

EYB

justify the use of the elastic model, and give additional information on intramultiplet and intermultiplet transitions. The transitions are found to be governed by the crossing of the two $\Omega = \frac{1}{2}$ potentials in the complex plane. The measured $I(\theta)$ and $I(\Theta)$ derived from the coupled-channel computations show small oscillations or perturbations (Stückelberg oscillations) though quantitative agreement is not obtained. The nature of the anomalous F - Xe $X\frac{1}{2}$ potential is discussed as is the approximation of a constant spin orbit coupling over the experimentally accessible range of internuclear distances for these open shell molecules.

Yuan T. Lee

ACKNOWLEDGEMENTS

One hundred thousand thanks to Professor Yuan T. Lee. His ability to communicate his physical insight, wide scientific knowledge, laboratory skill, and enthusiasm is greatly appreciated, as is his guidance, patience, and amiability.

I also wish to thank Drs. Piergiorgio Casavecchia, James Valentini, and Peter Tiedemann with whom I've had the pleasure to work with on several projects. Thanks also go to Drs. Ron Olson, William Lester, Jr., and Robert Walker for their guidance and assistance with much of the theoretical and computation aspects of my work here. Thank you to the group members past and present for their teaching, stimulating discussions, and friendship: Cheuk Ng, Michael Coggiola, Trudy Schafer, James Farrar, Andy Wang, Richard Buss, Randy Sparks, Matthew Vernon, Sylvia Ceyer, Carol Kahler, Florence Lin, Marta Kowalczyk, Kosuke Shobatake, Steve Sibener, Peter Schulz, Aasmund Sudbø, Ed Grant, Manfred Faubel, Dennis Trevor, Carl Hayden, Lee Carlson, Sandy Bustamente, Scott Anderson, Doug Krajnovich, Dieter Gerlich, Dan Neumark, Hoi-Sing Kwok, and Tomohiko Hirooka, as well as two chemistry friends outside the group, Erwin Poliakoff and Dana Dlott.

Thanks go to Ms. Ann Weightman for her preparation of the manuscript and patience with my many corrections, Allan Susoeff for his machining and engineering skills, and all the other people giving technical and machining support.

My warmest appreciation for my family, big neighborhood friends, and friends of the Empty Gate Zen Center for their joy, teaching, patience, and encouragement during the course of this work.

This work has been financially supported by the Office of Naval Research (Contract No. N00014-77-C-0101), and by the Division of Chemical Sciences, Office of Basic Energy Sciences, U. S. Department of Energy under contract no. W-7405-Eng-48.

COLLISIONS OF HALOGEN (^2P) AND RARE GAS (^1S) ATOMS

Contents

I. CROSSED MOLECULAR BEAM STUDIES ON THE INTERACTION POTENTIAL FOR $F(^2P) + Xe(^1S)$ 1

Introduction 1

Experimental 3

Results and Analysis 4

Discussion 11

References 13

Tables 16

Figure Captions 17

Figures 18

II. CROSSED MOLECULAR BEAM STUDIES ON THE INTERACTION POTENTIALS FOR $F(^2P) + Ne,Ar,Kr(^1S)$ 22

Introduction 22

Experimental Method 25

Results and Analysis 27

Discussion 32

References 34

Tables 36

Figure Captions 37

Figures 38

III. CROSSED MOLECULAR BEAM STUDIES ON THE INTERACTION POTENTIALS FOR $Cl(^2P) + Xe(^1S)$ 45

Introduction 45

Experimental 46

Results and Analysis 47

Discussion 50

References 53

Tables 54

Figure Captions 55

Figures 56

IV. COUPLED-CHANNEL STUDY OF HALOGEN (^2P) + RARE GAS (^1S) SCATTERING 58

Introduction 58

Theory 60

A. Scattering 60

B. Interaction Potentials 65

Results 69

A. Numerical Considerations 69

B. F-Xe 73

C. F-Ar 77

D. Cl-Xe 79

Discussion 82

Summary and Conclusions 86

References 87

Tables 91

Figure Captions 95

Figures 97

I. CROSSED MOLECULAR BEAM STUDIES ON THE INTERACTION POTENTIAL FOR $F(^2P) + Xe(^1S)$

Introduction

Recently much work has focused on diatomic rare-gas halide molecules because they comprise a new class of lasers in the near to vacuum ultraviolet region. Spontaneous emission and laser action from many of the rare gas-halide (RG-X) combinations have now been reported.[1] The ground state RG-X interactions themselves are also of fundamental chemical interest. The lack of detailed information on RG-X interaction potentials, in the past, made it difficult to evaluate the theoretical understanding of the termolecular recombination of halogen atoms in a rare gas environment. The lasing excited states seem rather well described by an ionic model,[2] and the effect of the spin-orbit interaction amongst these states has been clearly detailed in ab initio calculations by Hay and Dunning.[3] The lower electronic manifold interactions ($^2P_{3/2,1/2} + {}^1S_0$) are not as simply described. Usually the potential energy curves are said to exhibit repulsive or van der Waals character;[4] yet the two curves arising from the energetically lower $^2P_{3/2} + {}^1S_0$ asymptote are significantly split.[3,4] This splitting can be explained in simple terms by the amount of electron overlap due to the different orientations of the halogen p orbitals. However it is also thought that for some systems (especially XeF and XeCl) there may be significant charge transfer involved in the ground state binding. An indication of this fact comes from the observation of

bound-bound emission in the XeF and XeCl spectra. Particular effort has been paid to the XeF system and the potential energy curves involved in the laser emission have been derived spectroscopically.[5,6] The most detailed spectra contain rotational as well as vibrational structure affording an internuclear distance estimate in addition to the well depth for the ground state and two strongly fluorescing states.[5c]

Experiments involving the decomposition of $FXe.SO_2F$ and $XeF^+OsF_6^-$ suggested the processes occurred via XeF formation; an estimate of a XeF binding energy of ~20 kcal/mole has been made.[7] Support for an estimate of ~10 kcal/mole came from studies suggesting a XeF role in the oxidation of NO and NO_2,[8] and H_2O[9] by XeF_2. Also the observation of XeF was reported in an electron spin resonance spectrum, the sample being a γ radiation damaged XeF_4 single crystal;[10] this study described the XeF as a σ-electron radical.

The XeF ground state, denoted $X^2\Sigma^+_{1/2}$ ($X\ \frac{1}{2}$) in Hund's case b (c) has attracted attention for several ab initio and semi-empirical calcalulations.[3b,4,11] Because of the large number of electrons involved, even with a "state of the art" calculation, none of the curves computed compare satisfactorily in the well region with the spectra derived potential of Tellinghuisen et al.[5c]

Consequently, in an effort to investigate the attractive well of the XeF ground state interaction potential, we have carried out differential cross section measurements for F ($^2P_{3/2,1/2}$) scattered off Xe ($^1S_0$) at three collision energies.

Experimental

The basic experimental technique has been described elsewhere in detail.[12] Supersonic beams of xenon and fluorine atoms seeded in a rare gas carrier are crossed at 90° in a collision chamber maintained at ~3 × 10^{-7} torr. Fluorine atoms are detected as a function of in plane scattering angle by a triply differentially pumped rotatable quadrupole mass spectrometer.

The fluorine atoms are produced by thermal dissociation of F_2 in a resistively heated nickel oven/nozzle (typically at ~700°C). Under normal operating temperature and F_2 partial pressure we estimated[13] and confirmed experimentally about equal flux of F and F_2 from the source. The signal at m/e 19 due to the dissociative ionization of scattered F_2 flux presented the greatest uncertainty in the ^{19}F atom scattering data. After several angular scans at m/e 19 (typically counting for 30 to 60 seconds at each angle) the intensity at m/e 38 was measured and compared over the same angular range. This comparison, combined with the estimated m/e 38:19 ratio for F_2 in the mass spectrometer allowed a subtraction of the F_2 contribution to obtain a corrected angular distribution of scattered F atoms as a function of laboratory scattering angle, $I(\Theta)$, for $F + Xe$.

The F_2^+/F^+ ratio for F_2 was measured as a function of oven temperature in a temperature range where no signficant dissociation takes place, and these values are extrapolated to the operation temperature. Because $I(\Theta)$ of F_2 for the $F_2 + Xe$ scattering showed no oscillations at any observed angle, and had high intensity and large slope at small

angles, any resultant error in $I(\Theta)$ of F for F + Xe would be a skewing at angles less than ~10°. We estimate a maximum systematic error of ~10% based on the reproducibility of measured m/e 38:19 intensities. All reported $I(\Theta)$ are relative values.

The thermal F source at ~700°C contains the spin-orbit excited component $^2P_{1/2}$. Due to the 404 cm^{-1} splitting, the amount of electronic to translational relaxation in the supersonic expansion under present conditions is expected to be small; thus the F ($^2P_{1/2}$) contribution to the mixed beam is estimated by Boltzmann and degeneracy weights.

The three relative collisions energies, nominally 2.11, 10.5, 13.9 kcal/mole, were obtained with 99% Ar/1% F_2, 96.5% He/3% Kr/0.5% F_2, and 99% He/1% F_2 gas mixtures, respectively, from stagnation pressure of ~500 torr behind the nozzle at ~700°C. The pure Xe beam was kept at room temperature. Supersonic beam velocity peaks and distributions were measured by time-of-flight detection. Typical full width half maximum velocity spreads for F and Xe are both ~10%.

Results and Analysis

The experimental data of $I(\Theta)$ for F + Xe at three collision energies are shown in Fig. 1 along with error bars representing ± one standard deviation. The nominal collision energies are also shown. The angular distribution at the lowest energy displays practically no oscillatory structure, whereas the two higher energy $I(\Theta)$ show a

low amplitude, slow oscillation with a faster oscillation superimposed. The physical interpretation of these $I(\Theta)$ follow.

Inelastic cross sections in these experiments involving the electronic transition between F ($^2P_{3/2}$) and F ($^2P_{1/2}$) are expected to be much smaller than elastic cross sections because the spin-orbit splitting (Δ) constitutes an appreciable fraction of the relative collision energy (E_{rel}). The inefficiency of this electronic transition has been shown in a recent semiclassical calculation for $F + Xe$.[14] Therefore a simple elastic approximation is employed in the analysis of $I(\Theta)$. In this model the total differential cross section is written as a sum of elastic differential cross sections $\sigma_{X\frac{1}{2}}(\theta)$, $\sigma_{I\frac{3}{2}}(\theta)$, and $\sigma_{II\frac{1}{2}}(\theta)$ for the three states $X\frac{1}{2}$, $I\frac{3}{2}$, and $II\frac{1}{2}$, where each elastic differential scattering cross section in the center of the mass coordinate system, $\sigma(\theta)$, is calculated from the associated single channel scattering[15] employing the corresponding spherically symmetric interaction potential given as a function of internuclear distance:

$$\sigma_{tot}(\theta) = \sigma_{X\frac{1}{2}}(\theta) + \sigma_{I\frac{3}{2}}(\theta) + a\sigma_{II\frac{1}{2}}(\theta) \quad . \qquad (1)$$

The factor a (=0.55) represents the 22% contribution of F ($^2P_{1/2}$) in the beam of F atoms. The $X\frac{1}{2}$ and $I\frac{3}{2}$ states correlate with the $^2P_{3/2} + {}^1S_0$ asymptote, while $II\frac{1}{2}$ correlates with $^2P_{1/2} + {}^1S_0$. $\frac{1}{2}$ and $\frac{3}{2}$ following X, I, and II are Ω quantum numbers; Ω is the projection of the total electronic angular momentum along the molecular axis.

This approximation should serve the useful purpose of evaluating interaction potentials. We note, however, that this approximation cannot account for the fast oscillations in $I(\Theta)$ which are believed to show perturbations in the elastic scattering due to non-adiabatic coupling between the three electronic states. This interpretation of the fast oscillations follows from the observation that the spacing of these oscillations is inversely proportional to the relative velocity.[16]

For the comparison of interaction potentials with the experimental $I(\Theta)$ we first use a flexible analytic form to describe the potentials for the calculation of $\sigma_{tot}(\Theta)$. The $\sigma_{tot}(\Theta)$ is then transformed into the laboratory coordinate system to give a calculated $I(\Theta)$, taking into account velocity and angular spread of the beams and spatial resolution of the detector. Comparison of calculated $I(\Theta)$ with experimental $I(\Theta)$ provides the basis for evaluation of the interaction potentials.

In the analysis of experimental results, the interaction potentials $V(r)$ are chosen to be the flexible piecewise analytic form Morse-Morse-switching function - van der Waals (MMSV) given here for reference:

$$f(x) = V(r)/\varepsilon \qquad x = r/r_m \tag{2}$$

$$\begin{aligned}
f(x) &= \exp(2\beta_1(1-x)) - 2\exp(\beta_1(1-x)) , && 0 < x \leq 1 \\
&= \exp(2\beta_2(1-x)) - 2\exp(\beta_2(1-x)) \equiv M_2(x) && 1 < x \leq x_1 \\
&= SW(x) \cdot M_2(x) + (1 - SW(x)) \cdot W(x) && x_1 < x < x_2 \\
&= -C_{6r}x^{-6} - C_{8r}x^{-8} \equiv W(x) && x_2 \leq x < \infty
\end{aligned}$$

and

$$SW(x) = \frac{1}{2}\left[\cos\left(\frac{\pi(x - x_1)}{(x_2 - x_1)}\right) + 1\right] ,$$

where $C_{6r} = C_6/(\varepsilon r_m^6)$, and $C_{8r} = C_8/(\varepsilon r_m^8)$; ε and r_m are the depth and position of potential minimum. The usual cubic spline function is not used as it frequently produced a local maximum and minimum for the $V_{X\frac{1}{2}}(r)$ curve.

Since there is good reason to believe that the information on the attractive well of the $X\frac{1}{2}$ state derived from spectroscopic data by Tellinghuisen et al.[5c] is more reliable than other information available, the data analysis is started with a potential using their values of ε and r_m, and a morse β value is derived from the spectroscopic constant, ω_e.

In order to calculate the differential cross section, it is necessary to have information covering the full range of interaction potential probed at a given collision energy. This means in addition to the attractive portion of the potential curve. the high energy repulsive wall has to be added before comparison can be made. The repulsive wall of the potential is described by the inner morse function, characterized by β_1. Since the scattering data is the result of three interaction potentials, $X\frac{1}{2}$, $I\frac{3}{2}$, and $II\frac{1}{2}$, we also have to make reasonable estimates of the $I\frac{3}{2}$ and $II\frac{1}{2}$ potentials. Fortunately, data obtained at three different collision energies are sensitive to different regions and different states of interaction potentials; thus a very meaningful comparison between experimental $I(\Theta)$, and $I(\Theta)$ derived from a given set of potential curves is possible.

The $I\frac{3}{2}$ and $II\frac{1}{2}$ interaction potentials used in this work were assumed (a) to be very near the corresponding one electron richer rare gas pair Ne-Xe,[17] and (b) $V_{II\frac{1}{2}}(r) = V_{I\frac{3}{2}}(r) + \Delta$. Justification

is based on the closed shell-closed shell electronic configuration for the π symmetry, having the fully occupied fluorine p orbital along the internuclear axis (see reference 3b). Some slight adjustments to the corresponding Ne-Xe potential were made reflecting different polarizabilities[18,19] and electron spatial probabilities[20] going from Ne to F. Also the spin-orbit splitting, primarily associated with tightly bound core electrons, is approximated as constant over the range of internuclear distance probed.

The van der Waals C_6 constant is estimated by the Slater-Kirkwood formula[21] for effective number of electrons; polarizabilities were taken from the literature.[18,19] The C_6 constant of $I\frac{3}{2}$ is calculated to be larger than $X\frac{1}{2}$ state, reflecting its larger polarizability.[18] This implies a slow curve crossing for the $X\frac{1}{2}$ and $I\frac{3}{2}$ states at fairly large r. We note that the C_6 calculated for $X\frac{1}{2}$ has the long-range mixture of one-third $^2\Pi$ and two-thirds $^2\Sigma^+$ character,[3,14] while the $I\frac{3}{2}$ is purely $^2\Pi$. Though the $II\frac{1}{2}$ state asymptotically approaches two-thirds $^2\Pi$ and one-third $^2\Sigma^+$, we have used the C_6 of the $I\frac{3}{2}$ state in order to keep the same potential form for $I\frac{3}{2}$ and $II\frac{1}{2}$. This approximation should have no significant effect in the calculation and comparison of differential cross sections. The permanent quadrupole-induced dipole moment interaction, varying as R^{-8} at long range, contributes only a small fraction of the C_8 dispersion term,[22] which in turn has a small contribution compared to the C_6 term (dispersion only). The C_8 constant is estimated from the Ne-Xe C_8 constant.[19] Higher order constants are neglected due to their uncertainty and very small contribution.

With these initial assumptions for the $X\frac{1}{2}$ and $I\frac{3}{2}$, $II\frac{1}{2}$ potentials, the parameters ε, r_m, β_1, and β_2 were varied in an attempt to match the calculated with experimental $I(\Theta)$ at the three relative collision energies.

The use of the $V_{X\frac{1}{2}}(r)$ of Tellinghuisen et al. (i.e., $\varepsilon = 3.359$ kcal/mole, $r_m = 2.293$ Å, and $\beta_1 = \beta_2 = 7.47$) proved quite satisfactory, though a shift of a few degrees from the experimental data at two highest energies in the position of the slow oscillation maxima and minima in the $I(\Theta)$ was noted. Consequently, the $V_{X\frac{1}{2}}(r)$ derived here is modified slightly by altering β_1 and β_2 for a better $I(\Theta)$ fit, keeping ε and r_m the same. In adjusting β_1 and β_2, the width of the well was kept constant to within ~0.01 Å. It is not clear whether this slight improvement in the $X\frac{1}{2}$ potential is really significant, since the small difference is certainly within the limit of experimental uncertainties, especially the uncertainty in the experimentally determined collision energies. The original estimates for the $I\frac{3}{2}$ and $II\frac{1}{2}$ potentials were generally satisfactory and little change is made in deriving these potential parameters. The resulting potential parameters are listed in Table I.

$I(\Theta)$ sensitivity to the $V_{X\frac{1}{2}}(r)$ is quite good for the two highest energies, allowing an estimate of knowledge of the $V_{X\frac{1}{2}}(r)$ to within 5% by these methods. The sensitivity to the $V_{I\frac{3}{2}}(r)$ is not as good; its influence shows most clearly in $I(\Theta)$ fall-off behavior at small angles, especially for the lowest energy $I(\Theta)$. We assign a 15% measure of confidence to this potential near the attractive well.

Calculated I(Θ) from the derived potentials are plotted along with the data in Fig. 1. The calculated I(Θ) are scaled to the data by a constant scaling factor which is determined by the minimization of a chi(χ)-square goodness-of-fit measure. I(Θ) are averaged over the geometric resolution of the detector/beam arrangement in all calculations; one calculation at each nominal collision energy assumes mono-energetic beams (single Newton diagram) to display clearly the nature of the oscillations; the other calculated curves show the realistic effect of velocity averaging over 15 Newton diagrams. In the 10.5 and 13.9 kcal/mole I(Θ), the slow oscillations are rainbow and supernumerary rainbow oscillations produced by the $X\frac{1}{2}$ state. The 2.11 kcal/mole data show orbiting behavior for the $X\frac{1}{2}$ state.

In order to show both the sensitivity of this fitting procedure to given potentials, and how realistic other published XeF potentials are, we have presented additional velocity averaged calculations of I(Θ) in Fig. 2 derived from other potentials. The comparisons are made at low energy and one high relative collision energy. Dunning and Hay[3b] have presented potentials for all states of interest here. Using these as input, the I(Θ) are calculated and compared with the data. These I(Θ) are qualitatively in error, due to the absence of any appreciable well in the V(r). This is not unexpected from the type of calculation used by Dunning and Hay. Another recent XeF potential calculation[23] using a one-electron relativistic effective core potential does not significantly alter these potential curves.

As an example to show the sensitivity to the $I\frac{3}{2}$, $II\frac{1}{2}$ potentials, Fig. 2 also shows $I(\Theta)$ calculated from the $V_{X\frac{1}{2}}(r)$ of this work and the $V_{I\frac{1}{2},II\frac{3}{2}}(r)$ of Dunning and Hay. Significant deviation from experimental data is shown in the low energy $I(\Theta)$. Fig. 2 also depicts the deeper $X\frac{1}{2}$ potential put forth by Krauss and Liu,[11] combined with the $V_{I\frac{3}{2},II\frac{1}{2}}(r)$ derived in this work. This $X\frac{1}{2}$ potential is deep enough to produce orbiting at low energy, while at the high energy, the position of the rainbow maximum is severely displaced. All interaction potentials considered are shown in Fig. 3.

The contribution to $I(\Theta)$ by each of the potentials presented in Table I is shown in Fig. 4. The relative weights from Eq. (1) are used in the $I(\Theta)$ plots for all energies.

Discussion

Dunning and Hay[3b] estimate the ionic contribution in configuration interaction to the $X\frac{1}{2}$ state to be 9.2% for XeF. However, the fact that their $X\frac{1}{2}$ potential does not well represent the $V_{X\frac{1}{2}}(r)$ given here and by Teilinghuisen et al.,[5c] raises the question of the accuracy of this appraisal. Yet, to simply say that the $X\frac{1}{2}$ binding is due to, or characterized by charge transfer, may be somewhat misleading. It is not clear that a two center coulombic interaction picture is really appropriate. For example, the role of inter-atomic correlation, and its coupling to intra-atomic correlation, formidable and important problems, need careful assessment. The $X\frac{1}{2}$ state is not strongly

bound by ordinary chemical standards, but it is significant that the $V_{X\frac{1}{2}}(r)$ minimum position, r_m, lies about 1½ Å inside the strictly van der Waals-like $V_{I\frac{3}{2}}(r)$ minimum. Though a physical picture of the electronic open shell-closed shell binding in the $X\frac{1}{2}$ state of XeF is not complete, the quantitative determination of $V_{X\frac{1}{2}}(r)$ carried out in this work is found, corroborating the spectroscopically derived potential by Tellinghuisen et al.

The estimates of the interaction potentials for the $I\frac{3}{2}$ and $II\frac{1}{2}$ states over the experimentally probed thermal energy range presented here should be quite realistic. At very small r, these two states should coalesce into a single $^2\Pi$ state as the electronic orbital angular momentum becomes strongly coupled to the internuclear axis, dominating the spin-orbit coupling.[3,24] However, these experiments at relatively low collision energies do not sample these internuclear distances, and the additional complication of including separate repulsive wall descriptions for the $V_{I\frac{3}{2}}(r)$ and $V_{II\frac{1}{2}}(r)$ is not warranted here.

References

1. For emission see e.g., (a) L. A. Kuznetsova, Y. Y. Kuzyakov, V. A. Shpanskii, and V. M. Khutoretskii, Vestn. Mosk. Univ. Ser. II Khim 19, 19 (1964); (b) M. F. Golde and B. A. Thrush, Chem. Phys. Lett. 29, 486 (1974); (c) J. E. Velazco and D. W. Sester, J. Chem. Phys. 62, 1990 (1975); (d) J. Tellinghuisen, A. K. Hays, J. M. Hoffman, and G. C. Tisone, J. Chem. Phys. 65, 4473 (1976). For laser action, see e.g., (e) S. K. Searles and G. A. Hart, Appl. Phys. Lett. 27, 243 (1975); (f) J. J. Ewing and C. A. Brau, Appl. Phys. Lett. 27, 350 (1975); (g) C. A. Brau and J. J. Ewing, Appl. Phys. Lett. 27, 435 (1975).

2. J. J. Ewing and C. A. Brau, Phys. Rev. A12, 129 (1975); J. Tellinghuisen, J. M. Hoffman, G. C. Tisone, and A. K. Hays, J. Chem. Phys. 64, 2484 (1976); M. Krauss, J. Chem. Phys. 67, 1712 (1977).

3. (a) P. J. Hay and T. H. Dunning, J. Chem. Phys. 66, 1306 (1977); (b) T. H. Dunning and P. J. Hay, "The covalent and ionic states of the rare gas monofluorides," J. Chem. Phys. (in press).

4. D. H. Liskow, H. F. Schaefer, P. S. Bagus, and B. Liu, J. Am. Chem. Soc. 95, 4056 (1973).

5. (a) J. Tellinghuisen, G. C. Tisone, J. M. Hoffman, and A. K. Hays, J. Chem. Phys. 64, 4796 (1976); (b) J. Tellinghuisen, P. C. Telling-

huisen, G. C. Tisone, J. M. Hoffman, and A. K. Hays, "Spectroscopic studies of diatomic noble gas halides III," J. Chem. Phys. (in press); (c) P. C. Tellinghuisen, J. Tellinghuisen, J. E. Velazco, J. A. Coxon, and D. W. Setser, "Spectroscopic studies of diatomic noble gas halides IV," J. Chem. Phys. (in press).

6. A. L. Smith and P. C. Kobrinsky, J. Mol. Spectr. 69, 1 (1978).

7. N. Bartlett and F. O. Sladky, Comprehensive Inorganic Chemistry, (Pergamon Press, London, 1973), Vol. I, p. 250.

8. H. S. Johnston and R. Woolfolk, J. Chem. Phys. 41, 269 (1964).

9. V. A. Legasov, V. N. Prusakov, and B. B. Chaivanov, Russ. J. Phys. Chem. 42, 610 (1968).

10. J. R. Morton and W. E. Falconer, J. Chem. Phys. 39, 427 (1963).

11. M. Krauss and B. Liu, Chem. Phys. Lett. 44, 257 (1976).

12. P. E. Siska, J. M. Parson, T. P. Schafer, and Y. T. Lee, J. Chem. Phys. 55, 5762 (1971).

13. K. S. Pitzer and L. Brewer, Thermodynamics (McGraw-Hill, New York, 1961), Second edition, p. 672.

14. R. K. Preston, C. Sloane, and W. H. Miller, J. Chem. Phys. 60, 4961 (1974).

15. See, e.g., E. H. S. Burhop in Quantum Theory, D. R. Bates, editor (Academic Press, New York, 1961) Vol. I, Ch. 9. The elastic phase-shifts are calculated by Numerov integration for F + Xe at 2.11 kcal/mole collision energy; otherwise, JWKB phase-shifts are used in the fitting, though accuracy is checked by Numerov integration.

16. A somewhat similar situation is described by R. Düren, H. O. Hoppe, and H. Pauly, Phys. Rev. Lett. 37, 743 (1976).

17. C. Y. Ng, Y. T. Lee, and J. A. Barker, J. Chem. Phys. 61, 1996 (1974).

18. H. J. Werner and W. Meyer, Phys. Rev. A13, 13 (1976).

19. J. S. Cohen and R. T. Pack, J. Chem. Phys. 61, 2372 (1974).

20. C. Froese Fischer, At. Data 4, 301 (1972).

21. K. S. Pitzer, Adv. Chem. Phys. 2, 59 (1959).

22. Values for the fluorine atom permanent quadrupole moment are found in M. A. Gardner, A. M. Karo, and A. C. Wahl, J. Chem. Phys. 65, 1222 (1976), and F. H. Mies, Phys. Rev. A7, 942 (1973). The Xe polarizability is given in Ref. 19. The permanent quadrupole-induced dipole induction energy is calculated from J. O. Hirschfelder, C. F. Curtiss, and R. B. Bird, Molecular Theory of Gases and Liquids (Wiley & Sons, New York, 1954), p. 987

23. W. R. Wadt, P. J. Hay, and L. R. Kahn, J. Chem. Phys. 68, 1752 (1978).

24. See, e.g., G. Herzberg, Spectra of Diatomic Molecules (Van Hostrand Reinhold Co., New York, 1950) second edition; or F. Masnou-Seeuws and R. McCarrol, J. Phys. B7, 2230 (1974).

TABLE I. XeF potential parameters.

		$X\frac{1}{2}$	$I\frac{3}{2}$, $II\frac{1}{2}$
ϵ	(kcal/mole)	3.359	0.16
r_m	(Å)	2.293	3.80
β_1		8.5	7.5
β_2		6.8	6.0
X_1		1.102	1.116
X_2		1.950	1.500
C_6	(kcal/mole·Å^6)	703.	750.
C_8	(kcal/mole·Å^8)	3740.	3740.

Figure Captions

Fig. 1. Laboratory angular distributions of scattered F for the $F(^2P) + Xe(^1S)$ system at three collision energies. Solid curves are calculated from best fit potentials of Table I, averaging over angular and velocity distributions of experimental conditions. Dashed curves show single Newton diagram calculations, averaging over experimental angular resolution.

Fig. 2. Sensitivity of calculated laboratory angular distributions of F from $F(^2P) + Xe(^1S)$ to given potentials. The $I(\Theta)$ are calculated according to Eq. (1) from: (a) $X\frac{1}{2}$, $I\frac{3}{2}$, and $II\frac{1}{2}$ potentials of Ref. 3b; (b) $X\frac{1}{2}$ potential of Table I, and $I\frac{3}{2}$ and $II\frac{1}{2}$ potentials of Ref. 3b; (c) $X\frac{1}{2}$ potential of Ref. 11, and $I\frac{3}{2}$ and $II\frac{1}{2}$ potentials of Table I. The data are shown for comparison.

Fig. 3. Interaction potentials of $F(^2P_{3/2}) + Xe(^1S_0)$; the solid line (——) represents present work (see Table I); × (TTVCS) from Ref. 5c; ○ (KL) from Ref. 11; □, Δ (DH) from Ref. 3b. Note the scale change at V(r) higher than 1 kcal/mole.

Fig. 4. Relative contribution to $I(\Theta)$ (single Newton diagram calculations) of each of the potentials of Table I at three collision energies according to Eq. (1).

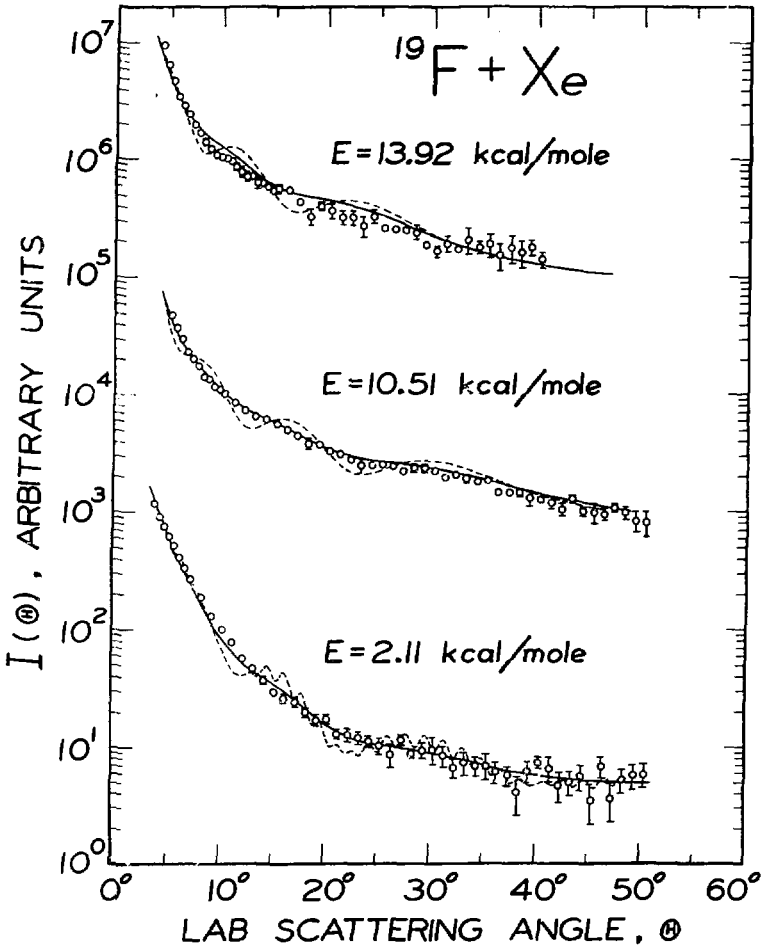

Fig. 1

XBL 784-8182 A

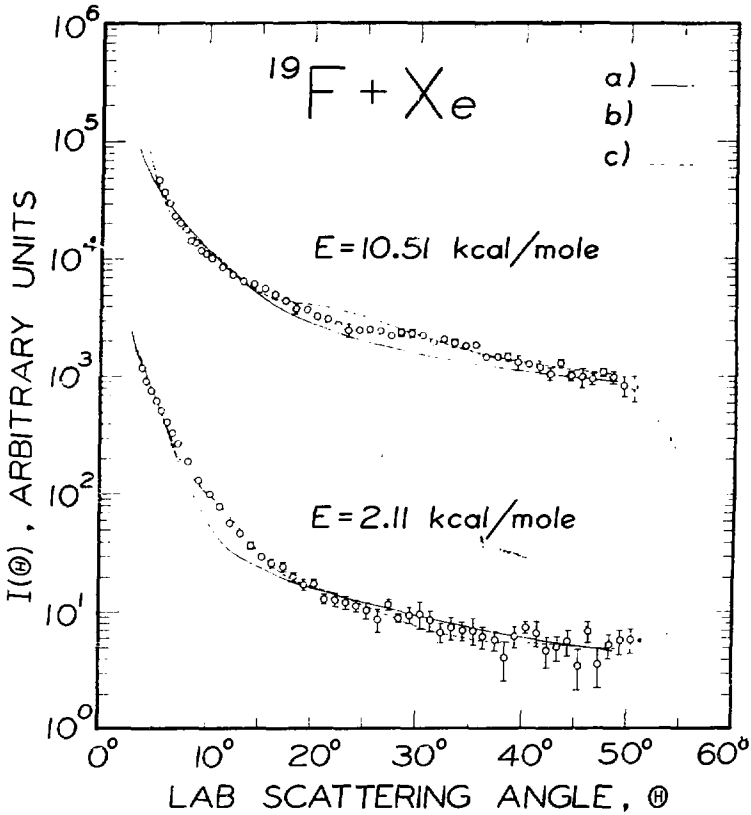

Fig. 2

XBL 784-8316

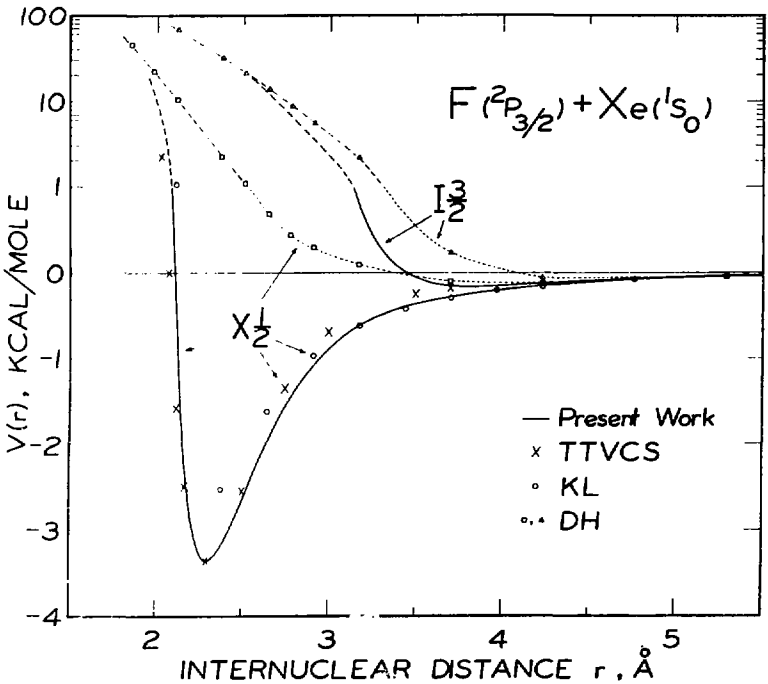

XBL 784-8315

Fig. 3

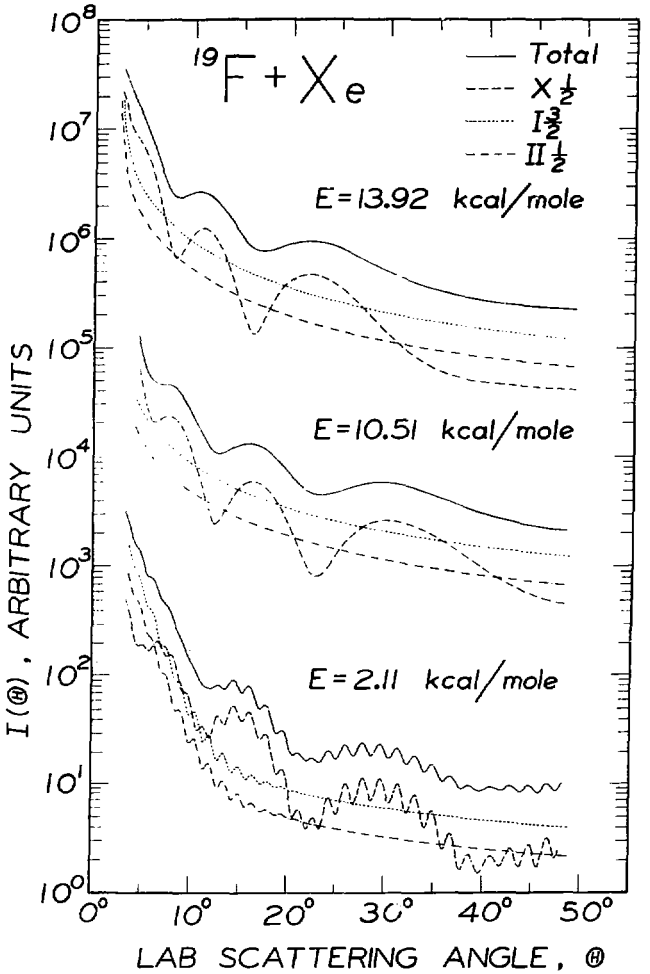

Fig. 4

XBL 784-8382

II. CROSSED MOLECULAR BEAM STUDIES ON THE INTERACTION POTENTIALS FOR $F(^2P)$ + Ne, Ar, $Kr(^1S)$

Introduction

Rare gas-monohalide molecules (RG-X) have received much attention recently, primarily due to their serving as the active medium in high power ultraviolet lasers. These lasers may be spectrally tuned[1] and Raman shifted,[2] pointing to their importance as ultraviolet photon sources. Lasing has been observed for KrF[3] and ArF,[4] while, to our knowledge, only spontaneous emission has yet been reported for NeF.[5] The understanding of both the emission spectra and the kinetics of lasing action in an excited rare gas/halogen medium can be aided by knowledge of the ground state potential energy curves (arising from the $RG(^1S)$ and $X(^2P)$ atomic terms).

Some of the kinetics of the rare gas halide laser medium bring to mind an older interest in RG-X and halogen atom-closed shell molecule interactions associated with the development of theories of termolecular recombination.[6] Considerable work is still needed on this topic. Improved potentials for ground state RG-X can be part of the basis of tests for models of recombination kinetics. In particular, care must be taken to account for the effect of multiple potential curves or surfaces[7] in systems containing open shell atoms.

Ab initio configuration interaction calculations carried out recently by Dunning and Hay[8] on the ground and excited state manifolds of the rare gas-monofluorides give a clear overview of the nature of the covalent and ionic bonding, including spin orbit interaction, for

all states of immediate interest. Dispersion forces are not accounted for in these computations and none of the ground state curves, including XeF, show any bonding. The analysis of spectroscopic data[9,10] and molecular beam differential scattering cross sections,[11] however, indicate XeF has a potential well depth of about 3.4 kcal/mole which is much deeper than might be expected for a van der Waals molecule. Another earlier computation by Krauss and Liu[12] for XeF $X^2\Sigma^+$ shows that a first order wavefunction including charge transfer, together with reasonable estimates of the interatomic correlation energy, can yield an appreciable well. At large internuclear separations the interatomic correlation energy becomes the familiar dispersion energy. No spin orbit interaction was included in the calculation.

But on the other hand, while XeF displays bound-bound emission terminating in the ground state, KrF exhibits only a bound-free spectra suggesting there must be a significant qualitative difference between ground state XeF and KrF. There still remains a need for further elucidation of these ground state electronically open shell-closed shell interactions. Hence, in an attempt to better understand the RG-X ground state interaction in the vicinity of the attractive well, and provide information pertinent to RG-F lasers and recombination studies, we have measured the differential cross sections of $F(^2P_{3/2,1/2})$ scattered off Ne, Ar, and $Kr(^1S_0)$ in the thermal energy range.

The derivation of interaction potentials from scattering data for systems containing non-S state open shell atoms is complicated and is often limited from the fact that there are more than one

potential energy curve involved in the scattering. But since the contributions from different potential energy curves to differential cross sections is a strong function of collision energy, it is possible to obtain meaningful conclusions if differential cross sections are carefully measured at several collision energies covering a wide energy range--and if the nonadiabatic coupling is weak (as in this case).

Experimental Method

The crossed beam apparatus has been described elsewhere[13] and the particular arrangement for F-RG scattering is nearly identical to that described for F-Xe,[11] with Ne, Ar, or Kr substituted for Xe. Very briefly, two supersonic beams are crossed at 90° under single collision conditions and scattered F atoms are detected in plane as a function of scattering angle by a rotating quadrupole mass spectrometer. The target beam is modulated at 150 Hz by a tuning fork chopper for background subtraction. The detector employs electron bombardment ionization of the neutral species prior to mass filtering. The detection efficiency of this method is proportional to the residence time of a particle in the ionizer; consequently the number density of scattered F atoms $I(\Theta)$ is measured, not the flux.

A minimum of 4 angular scans of $I(\Theta)$ were taken for each system, at each energy. The collision energy was varied by adjusting the F velocity by changing the composition of the fluorine atom rare gas carrier, employing the seeded beam technique, and keeping the nozzle temperature at ~700°C. The target rare gas was a pure beam at room temperature. The fluorine gas mixture composition and nominal collision energies (in kcal/mole) are as follows: for 99% Ar/1% F_2, 1.98 F-Ar, 2.07 F-Kr; for 69.5% He/30% Kr/0.5% F_2, 2.21 F-Ne, 2.50 F-Ar, 2.72 F-Kr; and for 99% He/1% F_2, 8.79 F-Ne, 11.1 F-Ar, 13.1 F-Kr. Typical velocity spreads for both beams determined by time-of-flight method are 10% full width at half maximum.

As the $F(^2P)$ spin orbit splitting (404 cm^{-1}) constituted a sizeable fraction of the collision energy, the inelastic process is expected

to be a very small contribution. Therefore, no attempt was made to detect the fine structure transition by analyzing the velocity of scattered F atoms.

Results and Analysis

Plots of the measured $I(\Theta)$ are presented on a semi-log scale in Figs. 1, 2 and 3. The lab angle Θ represents the scattering angle away from the F beam, toward the RG beam. The $I(\Theta)$ are given in relative units. For each system a reference angle Θ_r was chosen (usually 10°) where the scattered signal was relatively strong; throughout the angular scans the $I(\Theta_r)$ was frequently measured to correct for drift in beam intensities. Error bars represent $\pm 1\sigma$ where

$$\sigma^2 = \sum_{i=1}^{N} (I_i - \bar{I})^2/(N - 1) \quad .$$

N, the number of measurements, varies from 4 to 7, so typically this represents 90 to 95% confidence limits.[14]

As previously described,[11] the fluorine atom source produces F_2 and $F(^2P_{1/2})$ in addition to $F(^2P_{3/2})$. The F_2 contribution to F^+ signal was subtracted to give the final $I(\Theta)$, and the analysis considers the $F(^2P_{1/2})$ contribution to $I(\Theta)$ to be 22% estimated by Boltzmann statistical weights corresponding to the fluorine nickel oven/nozzle temperature of 700°C.

The approximate scheme of analysis to obtain potential curves by fitting the $I(\Theta)$ is the same as that of Ref. 11. We summarize this method as follows. Using Hund's case c notation the $F(^2P_{3/2}) + RG(^1S_o)$ four-fold degenerate asymptote splits into two doubly degenerate states at shorter internuclear distances: the X 1/2 (or I 1/2) and I 3/2. The $^2P_{1/2} + {}^1S_o$ asymptote gives rise to the doubly degenerate II 1/2 state. In this notation the 1/2 or 3/2 represents the Ω quantum number (the projection of the total electronic angular momentum upon the

internuclear axis); the X, I, II represents the energy ordering of the states, X or I being the lowest in energy. A flexible analytic form (Morse-Morse-switching function-van der Waals) is employed for the interaction potential energy V(r):

$$f(x) = V(r)/\varepsilon \qquad x = r/r_m \tag{1}$$

$$\begin{aligned} f(x) &= \exp(2\beta_1(1 - x)) - 2\exp(\beta_1(1 - x)) \;, && 0 \leqslant x \leqslant 1 \\ &= \exp(2\beta_2(1 - x)) - 2\exp(\beta_2(1 - x)) \equiv M_2(x) && 1 < x \leqslant x_1 \\ &= SW(x)\cdot M_2(x) + (1 - SW(x))\cdot W(x) && x_1 < x < x_2 \\ &= -C_{6R}x^{-6} - C_{8R}x^{-8} \equiv W(x) && x_2 \leqslant x < \infty \end{aligned}$$

and

$$SW(x) = 1/2\left[\cos\left(\frac{\pi(x - x_1)}{(x_2 - x_1)}\right) + 1\right] \;,$$

where $C_{6R} = C_6/\varepsilon r_m^6$, $C_{8R} = C_8/\varepsilon r_m^8$, and ε and r_m are the depths and position of the potential minimum. Using the approximation $V_{II\ 1/2} \simeq V_{I\ 3/2}$, the center of mass differential cross section $\sigma(\theta)$ is computed for each state independently by partial wave analysis assuming a spherically symmetric interaction; then each state's contribution is given its appropriate statistical weight and added to give a total $\sigma_T(\theta)$. For the 22% $^2P_{1/2}$ contribution this becomes

$$\sigma_T(\theta) = 1/2(0.78)[\sigma_{I\ 1/2}(\theta) + \sigma_{I\ 3/2}(\theta)] + (0.22)\ \sigma_{II\ 1/2}(\theta) \;. \tag{2}$$

We term this procedure a case c elastic approximation. A given $\sigma_T(\theta)$ is transformed[15] into the lab frame to give an $I(\Theta)$. Weighted sums of $I(\Theta)$ are taken for various collision energies corresponding to

the finite beam velocity spreads, and finally, the energy averaged $I(\Theta)$ is angular averaged over the beam/detector geometry and scaled to the data for direct comparison. By varying the parameters of the $V(r)$'s we attempt to find a best fit to the data and so obtain the $V(r)$'s.

The accuracy of this case c elastic approximation is supported in two ways. First, for the case of F-Xe where a spectroscopically determined potential was available,[9,10] this scattering method gave results ($V_{X\ 1/2}(r)$) in agreement[11] with the earlier published results. Second, rigorous coupled-channel states scattering computations[16] show that the elastic approximation reproduces very well all the gross features of the $I(\Theta)$ for the range of systems and energies studied.

The potential parameters for the derived interaction potentials are listed in Table I and the potentials are depicted in Figs. 4-6. These potentials can be considered valid to about 8 kcal/mole on the repulsive wall due to the range of collision energies studied.

Some remarks on the $I(\Theta)$ are appropriate. At even the lowest collision energies, no scattering rainbows are fully resolved. A significant portion of the rainbow on the dark side is seen for the F-Ar and F-Kr data, whereas the F-Ne $I(\Theta)$ resembles an almost hard sphere scattering. In contrast to the F-Xe data,[11] this shows that the strength of interaction for the F-Ne, Ar, Kr is considerably less than for F-Xe. Also the F-Ar and F-Kr $I(\Theta)$ show very nearly the same shape indicating quite similar potentials for the two systems. The wide angle scattering for the F-Ar 1.98 kcal/mole data is noisy; it is felt not to be as trustworthy. Because rainbow features are not fully

resolved in these systems there is less information for the analysis, and the resulting potentials are less well known than for F-Xe.

Estimates of the uncertainties in ε and r_m were obtained by making a matrix of plots of computed $I(\Theta)$, with the different matrix elements corresponding to potentials with differing (ε, r_m) values (always keeping the overall potentials to a reasonable shape). The ε, r_m values were varied for different states until the fits to the lab $I(\Theta)$ became poor. These matrices of computed $I(\Theta)$ were constructed at 2 energies per system. The resultant uncertainties are, for F-Ar and F-Kr, $\pm 10\%$ for the X 1/2 state's ε and r_m, and for the I 3/2, II 1/2 states $\pm 20\%$ in ε and $\pm 15\%$ in r_m. For F-Ne, uncertainties are for all states $\pm 25\%$ in ε and $\pm 15\%$ in r_m. While the Morse parameters governing the shape of the potential near the minimum and the repulsive wall were not varied in this systematic fashion, it is felt from the trial and error fitting that the uncertainties in their values are of a similar magnitude.

The long range C_6 constants were estimated by the Slater-Kirkwood formula[17] for effective number of electrons; polarizabilities were taken from the literature.[18,19] The I 3/2 C_6 is taken according to π symmetry, while the I 1/2, II 1/2 C_6's can be taken as the averages of the π and Σ contributions (see Ref. 16, Eq. (13)). However, the C_6 for the II 1/2 was set equal to that of the I 3/2 for ease in analysis. This should have a negligible effect. The C_8 constants were estimated from the Ne-Ne, Ar, Kr C_8 constants.[19] The permanent quadrupole-induced dipole R^{-8} contribution is small compared to the dispersion C_8 and was ignored, as were higher asymptotic terms due to their small size and uncertainty. The x_2 joining points used were slightly larger than the cut-off point

$2\left(\langle r_F^2\rangle^{1/2} + \langle r_{RG}^2\rangle^{1/2}\right)$ which has been suggested[20] for the validity of the power series expansion. The x_2 values used gave better $I(\Theta)$ fits, and after some trial calculations varying the x_2's, the quoted values were held fixed in the fitting. The C_6 and C_8 constants were not altered during the fitting.

Discussion

Due to the inherent difficulty of extracting information on multiple potential curves which scatter simultaneously, the effects of interstate coupling, and decreased signal to noise at large scattering angles, very accurate determination of repulsive walls of the potentials is precluded. Nevertheless, a comparison of the repulsive wall for F-Kr $V_{X\ 1/2}(r)$ with one previously determined by diffuse spectra simulation[21] shows reasonable accord. Ab initio calculations[8,22] undoubtedly are of more value in describing the repulsive walls away from the region of the small wells than these scattering results, if the spin orbit energy remains approximately constant with r. It is questionable that the F-Ne $V_{X\ 1/2}(r)$ is more repulsive than for F-Ar and F-Kr as shown in Fig. 7. Still, we believe these potential curves to be valid within the stated uncertainties. Of course, further improvements of experimental resolution, signal to noise ratio, and more collision energies studied, undoubtedly will provide more accurate information.

The X 1/2 potentials shown in Fig. 7 for F-Ne, Ar, Kr, Xe determined from these scattering studies do not follow a simple trend, as might have been expected. Obviously, this portrays a nonsimple interaction. The model described and computed by Krauss and Liu[12] offers a very plausible explanation of these surprising results. That is, the X 1/2 state well arises from a combination of some charge transfer character lessening the repulsion coming from Pauli exclusion, and the attractive interatomic correlation energy (the dispersion energy in the region of zero electron overlap). Apparently, it is a matter of the fine detail of the strengths of these interactions at given internuclear

distances which determine the shapes of the wells. Given that these interactions are to a good degree separable, this class of molecules may provide insight into the nature of interatomic correlation in regions of significant electron overlap.

However, as this model is not fully quantitative, it is still worthwhile to consider other contributions to the anomalous XeF X 1/2 potential well. Little is known about the relativistic spin orbit interaction for open shell molecules.[23] Given that the electrostatic Hamiltonian allows for close F-Xe approach with charge transfer, a changing unpaired electron character visible to the nuclei (especially Xe) might produce a significant negative energy contribution.

References

1. T. R. Loree, K. B. Butterfield, and D. L. Barker, Appl. Phys. Lett. 32, 171 (1978).

2. See, for example, J. R. Murray, J. Goldhar, and A. Szöke, Appl. Phys. Lett. 32, 551 (1978).

3. J. J. Ewing and C. A. Brau, Appl. Phys. Lett. 27, 350 (1975).

4. J. M. Hoffman, A. K. Hays, and G. C. Tisone, Appl. Phys. Lett. 28, 538 (1976).

5. J. K. Rice, A. K. Hays, and J. R. Woodworth, Appl. Phys. Lett. 31, 31 (1977).

6. For some different viewpoints, as well as literature review, see, G. Porter and J. A. Smith, Nature 184, 446 (1959); J. C. Keck, Adv. Chem. Phys. 13, 85 (1967).; D. L. Bunker, Theory of Elementary Gas Reaction Rates (Pergamon, Oxford, 1966), Chapter 4; W. H. Wong and G. Burns, J. Chem. Phys. 58, 4459 (1973); and E. E. Nikitin, Theory of Elementary Atomic and Molecular Processes in Gases (Clarendon Press, Oxford, 1974), Chapter 7.

7 D. G. Truhlar, J. Chem. Phys. 56, 3189 (1972); J. T. Muckerman and M. D. Newton, J. Chem. Phys. 56, 3191 (1972).

8. T. H. Dunning and P. J. Hay, J. Chem. Phys. 69, 134 (1978).

9. J. Tellinghuisen, P. C. Tellinghuisen, J. A. Coxon, J. E. Velazco, and D. W. Setser, J. Chem. Phys. 68, 5187 (1978).

10. A. L. Smith and P. C. Kobrinsky, J. Mol. Spectr. 69, 1 (1978).

11. C. H. Becker, P. Casavecchia, and Y. T. Lee, J. Chem. Phys. 69, 2377 (1978). (Chapter I)

12. M. Krauss and B. Liu, Chem. Phys. Lett. 44, 257 (1976).

13. P. E. Siska, J. M. Parson, T. P. Schafer, and Y. T. Lee, J. Chem. Phys. 55, 5762 (1971); J. M. Parson, P. E. Siska, and Y. T. Lee, J. Chem. Phys. 56, 1511 (1972).

14. D. P. Shoemaker, C. W. Garland, and J. I. Steinfeld, Experiments in Physical Chemistry (McGraw-Hill, NY, 1974), 3rd ed., pp. 32-34.

15. T. T. Warnock and R. B. Bernstein, J. Chem. Phys. 49, 1878 (1968).

16. C. H. Becker, P. Casavecchia, Y. T. Lee, R. E. Olson, and W. A. Lester, Jr. (to be submitted to J. Chem. Phys.). (Chapter IV)

17. K. S. Pitzer, Adv. Chem. Phys. 2, 59 (1959).

18. H. J. Werner and W. Meyer, Phys. Rev. A 13, 13 (1976).

19. J. S. Cohen and R. T. Pack, J. Chem. Phys. 61, 2372 (1974).

20. R. J. LeRoy, Molecular Spectroscopy (The Chemical Society, London, 1973), Vol. I, pp. 113-176.

21. J. Tellinghuisen, A. K. Hays, J. M. Hoffman, and G. C. Tisone, J. Chem. Phys. 65, 4473 (1976).

22. M. A. Gardner, A. M. Karo and A. C. Wahl, J. Chem. Phys. 65, 1222 (1976).

23. For some discussions on this subject see T. E. H. Walker and W. G. Richards, Phys. Rev. 177, 100 (1969); R. E. Smalley, D. A. Auerbach, P. S. H. Fitch, D. H. Levy, and L. Wharton, J. Chem. Phys. 66, 3778 (1977); R. Ahmad-Bitar, W. P. Lapatovich, D. E. Pritchard, I. Renhorn, Phys. Rev. Lett. 39, 1657 (1977); S.-T. Lee, S. Süzer, and D. A. Shirley, Chem. Phys. Lett. 41, 25 (1976).

Table I. F-Ne, Ar, Kr potential parameters for states (X 1/2), (I 3/2, II 1/2).

	F-Ne	F-Ar	F-Kr
ε (kcal/mole)	0.12,0.09	0.28,0.15	0.31,0.155
r_m(Å)	2.85,3.05	2.95,3.45	3.0,3.6
β_1	7.4,8.2	4.3,5.5	4.3,5.5
β_2	6.8,7.5	4.3,5.5	4.3,5.5
x_1	1.056,1.051	1.161,1.126	1.161,1.126
x_2	1.500,1.500	1.700,1.400	1.700,1.500
C_6 (kcal/mole·Å^6)	107.,113.	291.,305.	484.,507.
C_8 (kcal/mole·Å^8)	276.,276.	1270.,1270.	2250.,2250.

Figure Captions

Fig. 1. Laboratory angular distributions of scattered F for the $F(^2P) + Ne(^1S)$ system, at two collision energies. Circles are data points and the solid curve is calculated from the best fit parameters of Table I.

Fig. 2. Same as in Fig. 1, except for $F(^2P) + Ar(^1S)$.

Fig. 3. Same as in Fig. 1, except for $F(^2P) + Kr(^1S)$.

Fig. 4. Best fit X 1/2 and I 3/2 potential curves for $F(^2P_{3/2}) + Ne(^1S_0)$. Note scale change at 0.1 kcal/mole.

Fig. 5. Same as in Fig. 4, except for $F(^2P_{3/2}) + Ar(^1S_0)$.

Fig. 6. Same as in Fig. 4, except for $F(^2P_{3/2}) + Kr(^1S_0)$.

Fig. 7. Comparison of the X 1/2 interaction potentials for the F + Ne, Ar, Kr, Xe series. Note scale change at 1.0 kcal/mole.

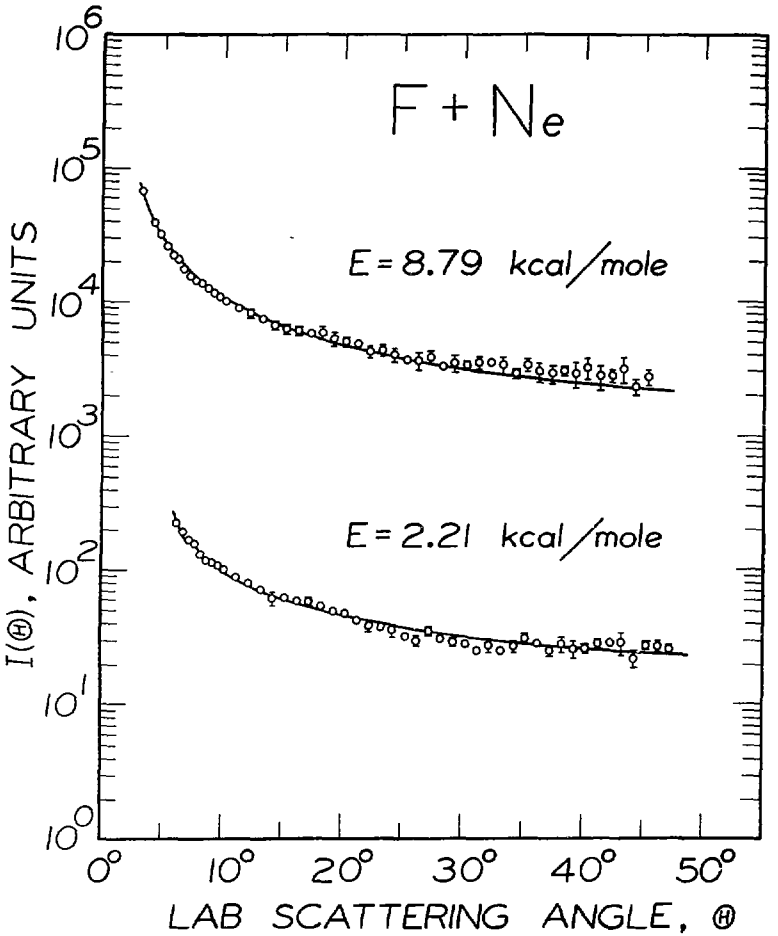

Fig. 1

XBL 786-9075

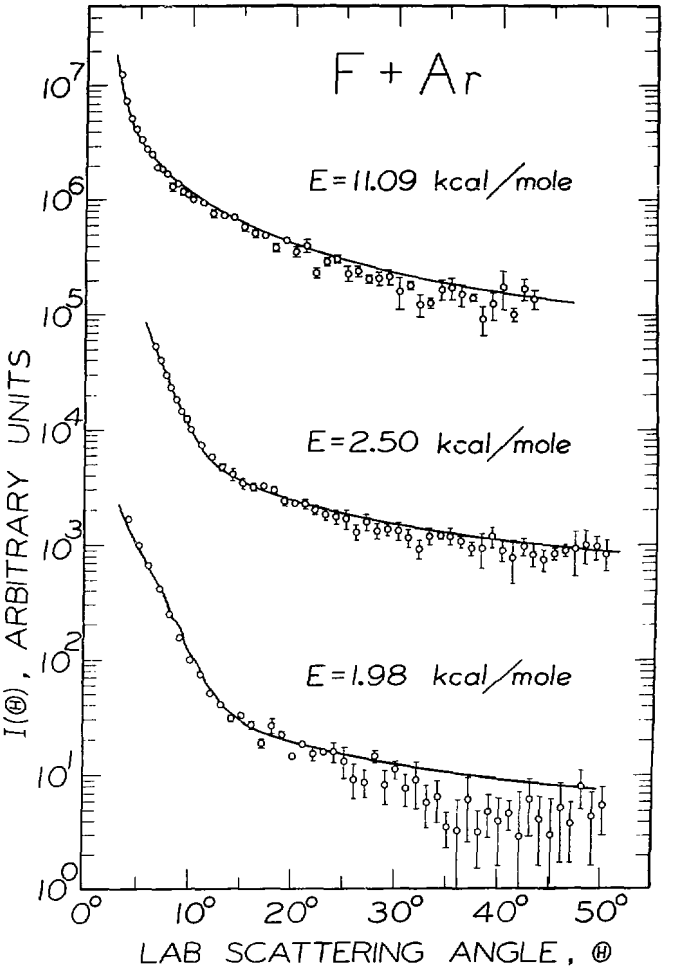

Fig. 2

XBL 786-9074

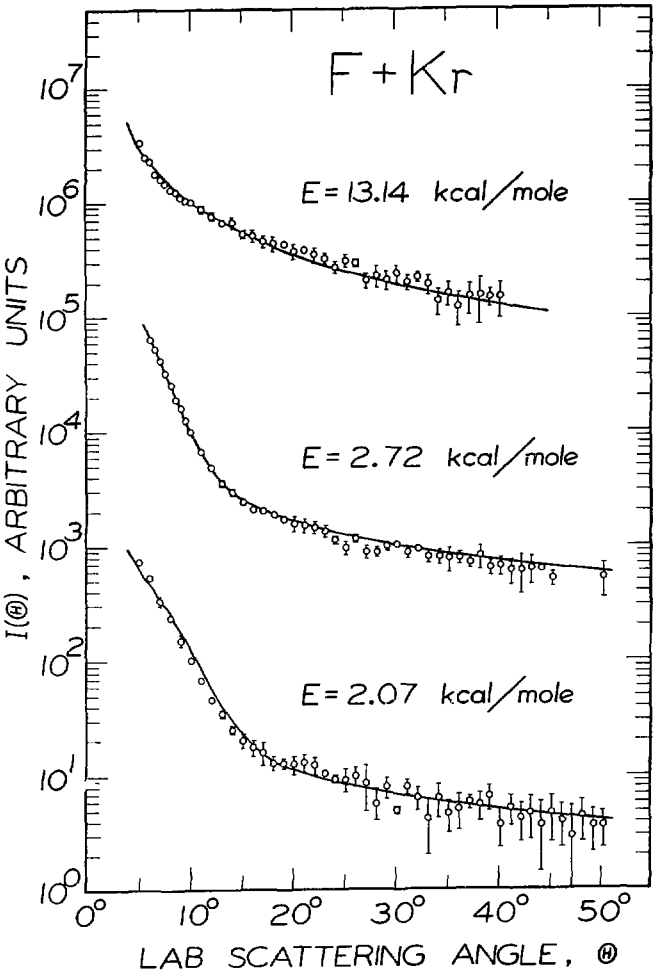

Fig. 3

XBL 786-9073

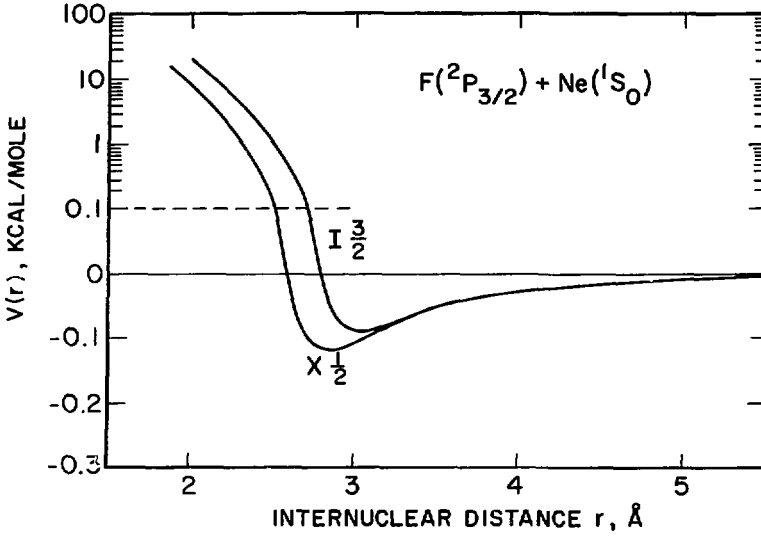

XBL 7810-12011

Fig. 4

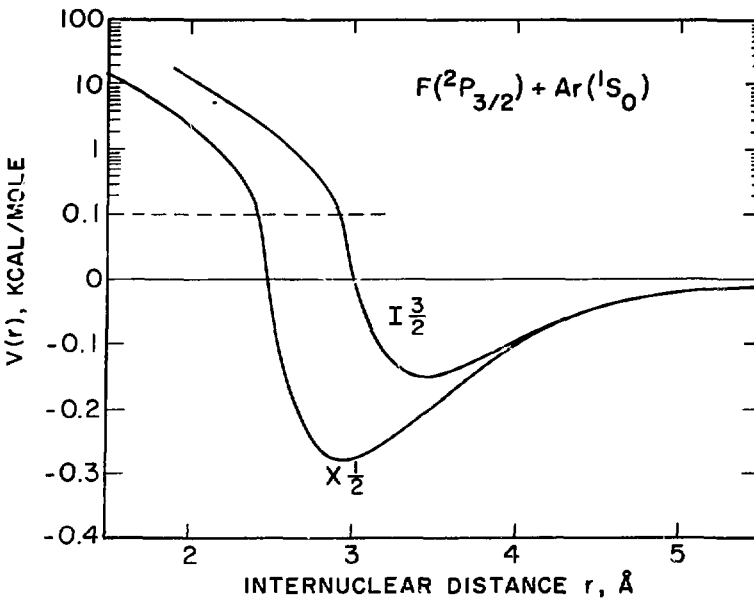

XBL 7810-12012

Fig. 5

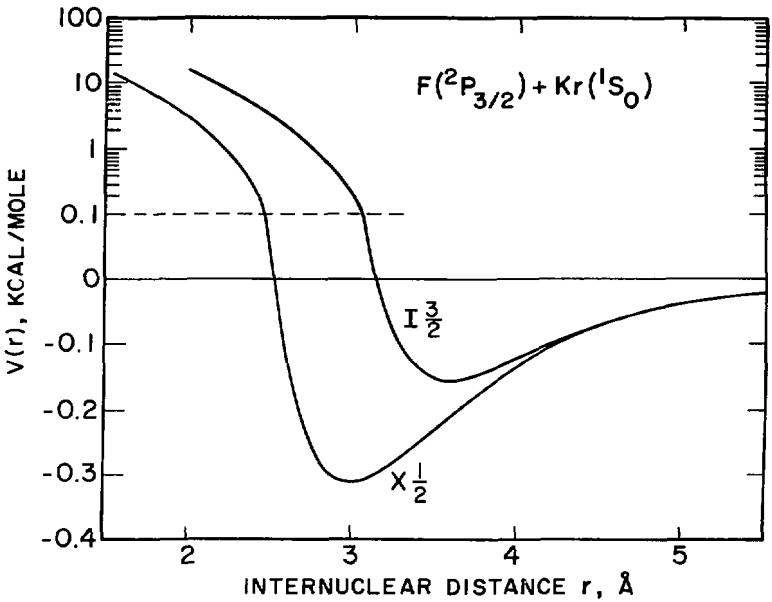

XBL 7810-12013

Fig. 6

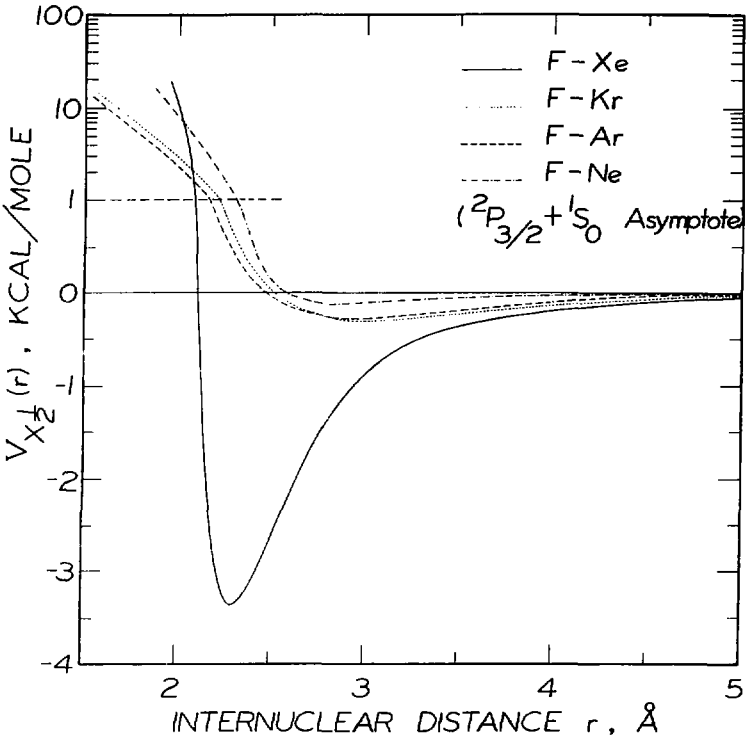

Fig. 7

XBL 786-9076

III. CROSSED MOLECULAR BEAM STUDIES ON THE INTERACTION POTENTIALS FOR $Cl(^2P) + Xe(^1S)$

Introduction

There has been considerable interest recently in halogen-rare gas (X-RG) diatomics as they comprise a class of high power ultraviolet excimer lasers. Cl-Xe was one of the first of these lasing systems (at 308 nm) to be reported.[1] In fact, excimer is somewhat a misnomer for the Cl-Xe, and F-Xe, systems, as bound-bound spectral transitions are observed. This has allowed accurate spectroscopic (RKR) analysis of the ground state $X\frac{1}{2}$ Cl-Xe potential.[2] No spectroscopic information is available for the $I\frac{3}{2}$ or $II\frac{1}{2}$ states, though ab initio configuration interaction calculations have been performed on all of the states of possible laser interest.[3] The state labels used throughout are those appropriate to Hund's case c coupling, and the electronic states considered in this work are the $X\frac{1}{2}$ (or $I\frac{1}{2}$) and $I\frac{3}{2}$ arising from the ground state fourfold degenerate $^2P_{3/2} + {}^1S_0$ atomic asymptote, and the $II\frac{1}{2}$ from the doubly denerate spin orbit excited $^2P_{1/2} + {}^1S_0$ asymptote. Knowledge of all these states is helpful in understanding the presence or absence of lasing transitions and kinetic details of the laser medium.

Hence, as a check on the Cl-Xe spectroscopically derived $X\frac{1}{2}$ potential $V_{X\frac{1}{2}}$, to obtain chemically accurate information on the $V_{I\frac{3}{2}}$ and $V_{II\frac{1}{2}}$, and as an example of the usefulness of scattering studies in giving quantitative information on adiabatic potentials not readily accessible to spectroscopic analysis, a crossed molecular beam experiment has been performed on $Cl(^2P) + Xe(^1S)$.

Experimental

The apparatus and technique used has been described in detail elsewhere.[4] After two stages of differential pumping, the Cl and Xe supersonic beams cross at 90° under single collision conditions in the scattering chamber maintained at ~3 x 10^{-7} torr. The Xe beam was modulated at 150 Hz by a tuning fork chopper for background subtraction. A triply differentially pumped rotating quadrupole mass spectrometer with electron bombardment ionizer and ion counter recorded the angular distributions I(Θ) of ^{35}Cl scattered by Xe. Counting times went from 10 to 80 sec per point depending on the signal count rate, and signals at a reference angle were used for the comparison of the signals at all the observed angles in order to normalize possible fluctuations of beam intensities and other experimental conditions.

The stagnation pressure and temperature of the Xe beam was kept at 450 torr and 20°C. With a 0.1 mm nozzle, this is about the highest stagnation pressure for Xe without significant dimer formation in the expansion. Cl atoms were produced by Cl_2 thermal dissociation in a resistively heated high density graphite oven/nozzle.[5] Different relative collision energies E_{rel} were obtained by varying the Cl velocity utilyzing the seeded beam technique. The gas mixtures used were ~1% Cl_2 in He, Ar, or Xe, and stagnation pressures ~1000 torr were used. No XeCl or $XeCl_2$ was found in the hot beam. Beam velocities and spreads were measured by the time-of-flight method, and the full-width-at-half-maximum (FWHM) velocity spreads were ~20% for Cl and ~10% for Xe. FWHM angular divergences were about 1° for Cl and 2° for Xe.

The graphite oven temperature of ~2000°K produces about 21% spin orbit excited $^2P_{1/2}$ atoms; the spin orbit relaxation of Cl atoms is expected to be very slow during the isentropic expansion. Consequently the composition of $Cl(^2P_{1/2})$ in the beam is not expected to differ from that in the oven. Some Cl_2 was also present in the beam and the small $^{35}Cl^+$ contribution from Cl_2 was taken into account from the measured angular distributions of Cl_2 detected as Cl_2^+ and the fragmentation ratio of $Cl_2(Cl^+/Cl_2^+)$ in the ionizer, and subtracted to give the final $I(\Theta)$ of Cl + Xe.

Inelastic scattering involving electronic transitions is expected to be a very small contribution to $I(\Theta)$ because of the large splitting of 881 cm^{-1} between $^2P_{1/2}$ and $^2P_{3/2}$ of Cl. Consequently no attempt was made to detect the fine structure inelastic process by time-of-flight.

Results and Analysis

Laboratory angular distributions of ^{35}Cl scattered off Xe are shown in Fig. 1 at nominal E_{rel} = 2.37, 2.57, 6.18, and 26.1 kcal/mole. Exemplary error bars are given, when visible outside the circles, representing ±1 standard deviation of the mean. The number of scans over an angular range varies from 3 to 9. As a check on the reproducibility of the data, the $I(\Theta)$ at E_{rel} = 2.57 kcal/mole was taken a considerable time after the other three $I(\Theta)$ were recorded using new beam set-ups intended for comparing $I(\Theta)$ at E_{rel} = 2.37. Although the collision energy turned out to be slightly higher, this data is compatible with the other $I(\Theta)$, as can be seen in Fig. 1.

An elastic scattering approximation is used in the analysis, which has been described elsewhere.[6] This method of computing differential cross sections neglects nonadiabatic coupling and is appropriate to molecules of Hund's case c coupling. JWKB phaseshifts are used in the single channel scattering. Twenty-one Newton diagrams contribute to final I(Θ) calculations to represent beam velocity spreads, and angular averaging is also performed to mimic the beam/detector geometry. Flexible piecewise analytic representations of the $V_{X\frac{1}{2}}$, $I\frac{3}{2}$ are used and the approximation $V_{II\frac{1}{2}} \simeq V_{I\frac{3}{2}}$ is employed. The potential form is the Morse-Morse-Hermite-spline-van der Waals (MMHV) function:

$$f(x) = V/\varepsilon \qquad x = r/r_m \tag{1}$$

$$\begin{aligned}
f(x) &= \exp(2\beta_1(1-x)) - 2\exp(\beta_1(1-x)) && 0 \le x \le 1 \\
&= \exp(2\beta_2(1-x)) - 2\exp(\beta_2(1-x)) && 1 < x \le x_1 \\
&= a_1 + (x-x_1)\cdot\{a_2+(x-x_1)\cdot[a_3+a_4(x-x_1)]\} && x_1 < x < x_2 \\
&= C_{6R}/x^6 - C_{8R}/x^8 && x_2 \le x < \infty
\end{aligned}$$

where $C_{iR} = C_i/(\varepsilon r_m^i)$, and ε and r_m are the depth and position of the potential minimum. Conditions on the Hermite spline are continuity of $f(x)$ and $\frac{df(x)}{dx}$ at x_1 and x_2. The C_6 constants are estimated from the Slater-Kirkwood formula for effective number of electrons;[7] polarizability values are from the literature.[8,9] The C_6 of $I\frac{3}{2}$ corresponds to π symmetry, while the C_6 of $X\frac{1}{2}$ is best approximated by the average of the Σ and π contributions (see Ref. 10, Eq. (13)). The C_8 is estimated from the Ar-Xe C_8.[9] The permanent quadrupole-induced dipole R^{-8} induction term is neglected because of its small size, as are other coefficients of the asymptotic expansion.

The $V_{X\frac{1}{2}}$, $I\frac{3}{2}$ are determined by fitting calculated I(Θ) to the experimental values through varying the analytic potential parameters. The C_6 and C_8 were held fixed though, and little variation was made in the x_1, x_2 values. Complete uniqueness of the fitted potentials is not guaranteed by this method. However, the range of the potentials are sensitive to the ratio of rainbow to wide angle scattering intensities. Rainbow and supernumerary rainbow positions and relative intensities are quite sensitive to potential well depths and curvature. To estimate these interaction potentials accurately it is necessary to measure the I(Θ) at several collision energies covering a wide range.

The validity of the elastic approximation is supported by its ability to corroborate an accurate spectroscopically determined $V_{X\frac{1}{2}}$ for F-Xe,[6a] and by more rigorous coupled-channel scattering calculations.[10]

The fitting began using an analytic representation of the spectroscopic numerical $V_{X\frac{1}{2}}$ values.[2a] It was found the experimental I(Θ) could not improve upon these values, so they were retained. Quite good sensitivity to the $V_{I\frac{3}{2}}$ well was found in the low energy I(Θ).

The final I(Θ) are shown in Fig. 1, the derived $V_{X\frac{1}{2}}$, $I\frac{3}{2}$ are shown in Fig. 2, and the potential parameters are listed in Table I. As already noted, the $V_{II\frac{1}{2}}$ can be approximated by the $V_{I\frac{3}{2}}$. In general though, a better $V_{II\frac{1}{2}}$ can be derived as shown in Ref. 10 from the $V_{X\frac{1}{2}}$ and $V_{I\frac{3}{2}}$.

The resultant $V_{I\frac{3}{2}}$ shows very close resemblance to the ground state $^1\Sigma$ Ar-Xe potential. Elastic scattering studies performed in our laboratory have given the Ar-Xe potential, which we believe to be accurate to ±3%

in ε and r_m.[11] The parameters of the Ar-Xe potential are also listed in Table 1 for reference. This Ar-Xe potential is slightly outside other recently proposed values.[12]

Uncertainties in the Cl-Xe ε and r_m parameters are obtained by systematically varying the parameters and observing when the I(Θ) fits become poor. The estimated maximum uncertainites are within ±7% in ε and r_m for both the $V_{X\frac{1}{2}}$, $V_{I\frac{3}{2}}$. Possible errors in the Morse β parameters are likely to be of a similar magnitude, based on their observed influence on the I(Θ) during the fitting procedure. Sensitivity to the repulsive walls is less than for the well region owing to worse signal-to-noise for the structureless wide angle I(Θ), and multiple potential scattering. Of course, there is no information gained about the repulsive wall above the highest E_{rel}.

Discussion

The I(Θ) measured in this experiment is the result of scattering of Cl with Xe through three interaction potentials. For this type of scattering experiment involving multiple interaction potentials, it is not possible to carry out meaningful analysis of individual potentials unless experiments are performed at many collision energies covering a wide energy range, and the coupling between different states involved is weak (as in this case).

The application of the elastic approximation for Hund's case c coupling, as previously done for F-Xe[6a] and F-Ne, Ar, Kr,[6b] again is fruitful in its corroboration of the recently obtained spectroscopic

$V_{X\frac{1}{2}}$[2a] and its yielding an accurate $V_{I\frac{3}{2}}$ (and $V_{II\frac{1}{2}}$). The spectroscopic $V_{X\frac{1}{2}}$ was not determined to an absolute r_m, but rather to a value relative to two excited states, though sound arguments were used in estimating r_m. While this study cannot place an extremely tight bound on the $X\frac{1}{2}$ r_m, again, it is supportive of the conclusions of Sur et al. We consider all our stated uncertainties to be conservative.

The fact that the obtained $V_{I\frac{3}{2}}$ is so similar to the Ar-Xe ground state potential underlines the validity of the electronic closed shell-closed shell van der Waals picture where the interaction takes place with the fully occupied p orbital along the internuclear axis. The greater strength of this van der Waals interaction as compared to the F-rare gas series has allowed the most accurate $V_{I\frac{3}{2}}$ well determination to date, simply due to its significant influence on the three lowest E_{rel} I(G).

The common explanation for the Cl-Xe $V_{X\frac{1}{2}}$ consists of a combination of (a) less repulsion due to only a half-filled p orbital along the internuclear axis, (b) a small amount of charge transfer lessening this repulsion, and (c) the contribution from interatomic correlation energy[13] (the dispersion energy in the limit of zero electron overlap). As has been mentioned,[6b] it may also prove worthwhile to examine the approximation that the spin orbit coupling is constant over the range of internuclear distances considered. It appears that Cl-Xe and F-Xe are the only two significantly bound X-RG molecules. However, the shapes (or force constants) of these two $V_{X\frac{1}{2}}$ are very different, F-Xe having a very tight well and Cl-Xe being broad. At this point, an explanation

of this phenomenon seems possible only by considering the absolute strengths of the above mentioned contributions as a function of internuclear distances.

Nonadiabatic coupling in XeCl and its influence on scattering is discussed in Ref. 10.

Finally, if there is a desire to extrapolate these repulsive walls to higher energy, one may make use ab initio calculations,[3] at least in obtaining the wall slopes. Alternatively, one may make use of the simple model recently proposed[14] to obtain Born-Mayer repulsion parameters from values of ε, r_m, and van der Waals coefficients, especially for the $V_{I\frac{3}{2}}$ and $V_{II\frac{1}{2}}$.

References

1. J. J. Ewing and C. A. Brau, Appl. Phys. Lett. 27, 350 (1975).

2. (a) A. Sur, A. K. Hui, and J. Tellinghuisen, (to appear in J. Mol. Spectr.); (b) J. Tellinghuisen, J. M. Hoffman, G. C. Tisone, and A. K. Hays, J. Chem. Phys. 64, 2484 (1976).

3. P. J. Hay and T. H. Dunning, Jr., J. Chem. Phys. 69, 2209 (1978).

4. P. E. Siska, J. M. Parson, T. P. Schafer, and Y. T. Lee, J. Chem. Phys. 55, 5762 (1971); Y. T. Lee, J. D. McDonald, P. R. LeBreton, and D. R. Herschbach, Rev. Sci. Instr. 40, 1402 (1969).

5. J. J. Valentini, M. J. Coggiola, and Y. T. Lee, Rev. Sci. Instr. 48, 58 (1977).

6. (a) C. H. Becker, P. Casavecchia, and Y. T. Lee, J. Chem. Phys. 69, 2377 (1978) (Chapter I); (b) C. H. Becker, P. Casavecchia, and Y. T. Lee, J. Chem. Phys. (in press) (Chapter II).

7. K. S. Pitzer, Adv. Chem. Phys. 2, 59 (1959).

8. E. A. Reinsch and W. Meyer, Phys. Rev. A 14, 915 (1976).

9. J. S. Cohen and R. T. Pack, J. Chem. Phys. 61, 2372 (1974).

10. C. H. Becker, P. Casavecchia, Y. T. Lee, R. E. Olson, and W. A. Lester, Jr. (to be submitted to J. Chem. Phys.). (Chapter IV).

11. C. H. Becker, R. J. Buss, and Y. T. Lee, Materials and Molecular Research Division, Lawrence Berkeley Laboratory, University of California, Annual Reports 1977 (LBL-7355), pp. 384-386.

12. G. C. Maitland and W. A. Wakeham, Mol. Phys. 35, 1443 (1978).

13. M. Krauss and B. Liu, Chem. Phys. Lett. 44, 257 (1976).

14. K. T. Tang and J. P. Toennies, J. Chem. Phys. 66, 1496 (1977); errata, ibid., 67, 375 (1977) and 68, 786 (1978).

Table 1. Cl-Xe $X\frac{1}{2}$, $I\frac{3}{2}$ and Ar-Xe $^1\Sigma$ Interaction Potential Parameters

	XeCl, $X\frac{1}{2}$	XeCl, $I\frac{3}{2}$	Ar + Xe
ε (kcal/mole)	0.80	0.37	0.379
r_m (Å)	3.23	4.10	4.01
β_1	5.2	7.6	6.5
β_2	3.3	5.1	6.33
C_6 (kcal/mole · Å^6)	2279.	2410.	1957.
C_8 (kcal/mole · Å^8)	14250.	14250.	12005.
C_{10} (kcal/mole · Å^{10})	---	---	93502.
x_1	1.2100	1.1162	1.1088
x_2	1.6500	1.3500	1.4500
a_1	-0.7500	-0.8000	-0.7519
a_2	1.6500	2.5216	3.1665
a_3	0.4434	2.0941	-5.5247
a_4	-2.5063	-13.6316	3.8055

Figure Captions

Fig. 1. Experimental number density angular distributions of ^{35}Cl scattered off Xe (circles), and best fit calculation (solid line) using the potential parameters of Table 1. Representative error bars are ±1 standard deviation of the mean.

Fig. 2. Cl Xe $X\frac{1}{2}$ and $I\frac{3}{2}$ interaction potentials. Note scale change at 0.1 kcal/mole.

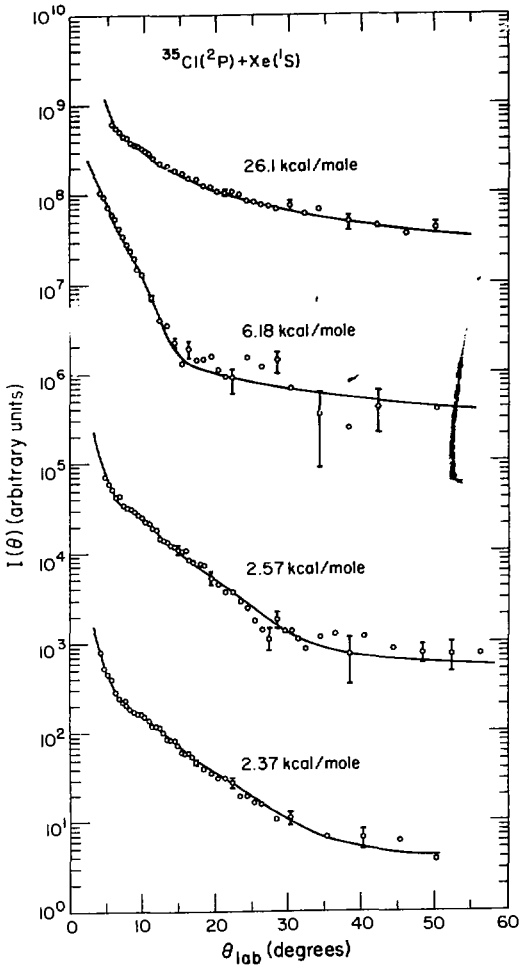
$^{35}Cl(^2P)+Xe(^1S)$
26.1 kcal/mole
6.18 kcal/mole
2.57 kcal/mole
2.37 kcal/mole
I (θ) (arbitrary units)
θ lab (degrees)
XBL 7811-12595

Fig. 1

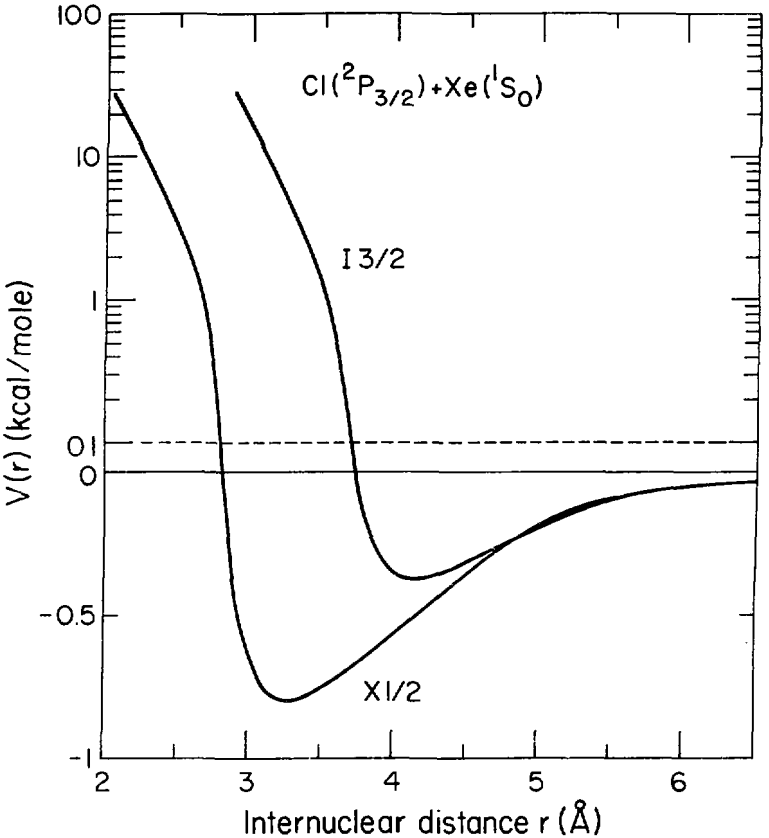

Fig. 2

XBL 7811-12584

IV. *COUPLED-CHANNEL STUDY OF* HALOGEN (^2P) + RARE GAS (^1S) SCATTERING

Introduction

The effects of the interaction of different neighboring electronic states on collision processes is a well studied topic with a half century history. Reflecting this is a vast literature, and reviews are available.[1] Many of the experimental studies have utilized fluorescence detection and dealt with collisions involving ^2P excited states of alkali atoms, with ground state rare gas atoms (RG), though other systems have been and are being investigated. Some recent examples of laboratory work can be found for depolarization of fluorescence (multipole cross sections),[2] fluorescence band shapes,[3] high resolution spectroscopy (via fluorescence) on supersonic beam produced molecules,[4,5] differential scattering cross sections by particle detection,[6-12] and integral inelastic cross sections via collision induced fluorescence.[13-15] The studies always focus on the adiabatic potentials V(R) as a function of internuclear distance R, and nonadiabatic coupling. Concommitant with this effort has been theoretical development, especially along semiclassical lines.[7,16] A rigorous quantum mechanical treatment for ^2P + ^1S scattering has been developed by Mies[17] and Reid,[18] and theory now exists for the case of two ^2P atoms or Σ state molecules.[19,20]

Because they permit simple computational approaches, elastic collision models [3,21] are especially useful in the analysis of experimental data. Discussion remains as to the accuracy of the models to predict total differential cross sections and integral inelastic cross sections. These formulations have focused on ^2P collisions of alkali atoms or C^+, systems with a single outer shell electron and small spin orbit splitting (Hund's case a or b). If the elastic approximation holds, it is possible

to extract valuable information on the interaction potentials by analyzing the laboratory differential cross sections $I(\Theta)$.

There is considerable need for ground state interaction potentials for rare gas-halides RG-X due to the development of RG-X ultraviolet lasers and for the theory of termolecular recombination of these systems (see, e.g., citations in Ref. 11). Although these states are not easily accessible to standard optical spectroscopy, it is possible from crossed atomic beam scattering experiments to measure total $I(\Theta)$ and, where the data are adequate, to extract the potentials from this data.

Though this study concerns again the familiar $^2P + {}^1S$ interaction, the spin orbit splitting Δ is large (0.0501 eV for F and 0.109 eV for Cl), and a Hund's case c coupling holds. An elastic approximation appropriate to this coupling case has been employed for F-Xe and appears successful since a potential derived from scattering data corroborates a spectroscopically determined potential.[10] If this approach is justified (and it appears it is) then accurate potentials can be obtained for ground state RG-X systems.[10-12] In turn, noting that both rigorous and approximate scattering models alike are quite sensitive to the V(R) used, these realistic V(R) can be the basis of more rigorous computations to yield detailed information unobtainable from an elastic model. Therefore, to both test this elastic approximation and obtain information on intra- and intermultiplet transitions among RG-X, quantum mechanical coupled-channel (CC) computations have been carried out employing the potentials derived from $I(\Theta)$ measured in crossed atomic beams experiments.

Theory

A. Scattering

Neglecting mass polarization terms and nuclear spin, which should have a negligible effect on the collision dynamics, the scattering problem reduces for each total angular momentum J to solution of a set of coupled radial Schrödinger equations[17,18]

$$\left[\frac{d^2}{dR^2} + k_j^2 - \frac{\ell(\ell+1)}{R^2}\right] F^J_{j\ell j'\ell'}(R) =$$

$$\frac{2\mu}{\hbar^2} \sum_{j''\ell''} V^J_{j\ell j''\ell''}(R) F^J_{j''\ell'' j'\ell'}(R) \quad . \qquad (1)$$

Here μ is the reduced mass, $k_j^2 = 2\mu/\hbar^2(E - E_j)$, and E is the total energy. The energy zero is chosen to be the $^2P_{1/2} + {}^1S_0$ asymptote, so that $E_{j=1/2} = 0$ and $E_{j=3/2} = -\Delta$, and $E - E_j = E_{rel}$ which is the relative kinetic energy.

The notation for the quantum numbers involved is as follows: j is the atomic angular momentum, m_j is the projection of j on a space fixed axis, Ω is the projection of j on the internuclear axis, ℓ is the nuclear orbital angular momentum, and J is the total angular momentum of the system. Primed (unprimed) quantities indicate final (initial) states. The molecular electronic states arising from the four-fold degenerate ground state $X(^2P_{3/2}) + RG(^1S_0)$ asymptote are the doubly degenerate I 1/2 (or X 1/2) and I 3/2 states. (In Hund's case b and a notation these are designated $^2\Sigma^+$ and $^2\Pi_{3/2}$, respectively.) From the doubly degenerate spin orbit excited manifold, $^2P_{1/2} + {}^1S_0$, one also obtains the II 1/2 state ($^2\Pi_{1/2}$ in Hund's case a). The 1/2, 3/2 are Ω values, and the

roman numerals indicate the energy ordering. Electronic states higher in energy than those already described are neglected because they lie considerably above the scattering energies investigated.

This set of coupled equations, Eq. (1), is derived in a space fixed frame and employs molecular adiabatic wavefunctions in constructing the total scattering wavefunction. Algebraically identical expressions for the interaction matrix elements $V^J_{j\ell j''\ell''}$ have been evaluated by Reid[18] and Mies[17] following slightly different approaches. The matrix elements $V^J_{j\ell j''\ell''}$ originate from the Born-Oppenheimer (BO) approximation and include the spin orbit interaction.[17] In writing Eq. (1), BO radial and rotational coupling terms (i.e., terms describing the breakdown of the BO approximation) have been omitted (see Ref. 17). The BO radial coupling terms here are likely to be smaller than for the strongly bound $F + H^+$ where Mies reasons they are negligible. Perturbation theory at large R for RG-X shows that the rotational BO coupling terms is $O(R^{-8})$ versus $V^J_{j\ell j''\ell''}$ $O(R^{-6})$; while at smaller R, again following Mies' arguments for the stronger $F + H^+$ interaction, the rotational term will be small compared to the elements of $V^J_{j\ell j''\ell''}$. Thus, these BO coupling terms have not been included.

The six open channels can be separated into two blocks according to parity,[17,18] resulting in the solution of Eq. (1) for two sets of three coupled equations.

Equations (1) were solved numerically by the log-derivative integration technique[22] to obtain the unitary and symmetric scattering matrices $\underset{\sim}{S}^J$, defined by the large R condition

$$F^J_{j\ell j'\ell'} \sim$$

$$\delta_{jj'}\delta_{\ell\ell'} \exp(-ik_jR - 1/2\ \ell\pi) - \left(\frac{k_j}{k_{j'}}\right)^{1/2} S^J_{j\ell j'\ell'}$$

$$\times \exp(ik_{j'}R - 1/2\ \ell'\pi) \qquad (2)$$

Differential cross sections for $j \to j'$ transitions can be conveniently constructed from the $\underset{\sim}{S}$ in the helicity representation[23] from

$$\frac{d\sigma(j \to j')}{d\omega} = (2j + 1)^{-1} \sum_{m_j = -j}^{j} \sum_{m_{j'} = -j'}^{j'} |f_{jm_j \to j'm_{j'}}(\Theta)|^2 \qquad (3)$$

where

$$f_{jm_j \to j'm_{j'}}(\Theta) = (-1)^{j+j'}(2ik_j)^{-1} \sum_J (2J + 1)\ d^J_{m_{j'}m_j}(\Theta)$$

$$\times \sum_{\ell\ell'} i^{\ell - \ell'} \begin{pmatrix} j' & J & \ell' \\ m_{j'} & -m_{j'} & 0 \end{pmatrix} \begin{pmatrix} j & J & \ell \\ m_j & -m_j & 0 \end{pmatrix}$$

$$\times [(2\ell' + 1)(2\ell + 1)]^{1/2} \left[S^J_{j\ell j'\ell'} - \delta_{jj'}\delta_{\ell\ell'}\right] ; \qquad (4)$$

the bracketed $\begin{pmatrix} \quad \end{pmatrix}$ quantities are Wigner 3j symbols. We followed Rose's phase convention[24] for the reduced rotation matrices.

The integral cross sections are evaluated by

$$\sigma(j \to j') = \frac{\pi}{(2j+1)\,k_j^2} \sum_{J\ell\ell'} (2J+1)\, |S^J_{j\ell j'\ell'} - \delta_{jj'}\delta_{\ell\ell'}|^2 \quad . \tag{5}$$

Integral cross sections with respect to specific m_j states $\sigma(jm_j \to j'm_j')$ are related to the $\sigma(j \to j')$ by

$$\sigma(j \to j') = \sum_{m_j m_j'} \frac{\sigma(jm_j \to j'm_j')}{(2j+1)} \quad , \tag{6}$$

and are computed using the most irreducible form[17,18b,25]

$$\sigma(jm_j \to j'm_j') = \sum_g (j,j',g|m_j,-m_j',m_j-m_j')^2\, B(j,j';g) \tag{7}$$

where g is a tensor order index, the $(j,j',g|m_j,-m_j',m_j-m_j')$ is a Clebsch-Gordan coefficient, and the Grawert B coefficients are given by

$$B(j,j';g) = \sum_\ell B_\ell(j,j';g) \tag{8a}$$

$$B_\ell(j,j';g) = \frac{\pi}{k_j^2} \sum_{\ell'} \left| \sum_J (-1)^{J+j'}(2J+1) \begin{Bmatrix} j & \ell & J \\ \ell' & j' & g \end{Bmatrix} T^J_{j\ell j'\ell'} \right|^2 \tag{8b}$$

where $\begin{Bmatrix} j & \ell & J \\ \ell' & j' & g \end{Bmatrix}$ is a 6j coefficient and $\underset{\sim}{T} = \underset{\sim}{I} - \underset{\sim}{S}$. The 36 cross sections are evaluated by 8 B coefficients (energy dependent). Multipole cross sections can be evaluated from the same coefficients.[2,18b,25]

The simple elastic approximation used for Hund's case c coupling[10] is given by

$$\frac{d\sigma_{el}(3/2 \to 3/2)}{d\omega} = 1/2\left[\frac{d\sigma_{I\ 1/2}}{d\omega} + \frac{d\sigma_{I\ 3/2}}{d\omega}\right] \quad , \tag{9a}$$

where the $d\sigma_i/d\omega$, $i \equiv I\ 1/2$, $I\ 3/2$, are computed following a single channel partial wave analysis. Consideration was given to an alternative expression, namely

$$\frac{d\sigma_{el}(3/2 \to 3/2)}{d\omega} = 1/2\ \left|f_{I\ 1/2}(\Theta) + f_{I\ 3/2}(\Theta)\right|^2 \quad , \tag{9b}$$

where the $f(\Theta)$ are scattering amplitudes for a single channel. Equation (9b) was suggested by an analogy to symmetrical resonance scattering[26] where two adiabatic potentials (gerade and ungerade states) share a common asymptote. Equation (9b) was found to poorly represent the experimental $I(\Theta)$ and CC calculated $d\sigma/d\omega$, and was not a good approximation. An objection to the analogy can be made on the following grounds. A physical picture for symmetric scattering is that transitions between the two states are constantly occurring over a very large range of internuclear distances. For the RG - X case, where $\Omega = 1/2$ and $3/2$ states correlate to the same $^2P_{3/2} + {}^1S_0$ asymptote, the total electronic Hamiltonian is diagonal in Ω within the BO approximation (see following section). Equation (9b) should also not be applied to the $\Omega = 1/2$ potentials since the interstate coupling is found to be localized and fairly weak (see Discussion). A semiclassical analysis[7] suited to this latter situation could be used for the $d\sigma/d\omega$ of the $\Omega = 1/2$ states but due to weak coupling, such complications are not warranted.

For comparison with the experimental $I(\Theta)$, the relatively small $^2P_{1/2}$ component (~20%) present in the beam is included in the analysis by use of the expression

$$\frac{d\sigma_{el}}{d\omega} = 1/2(0.8)\left[\frac{d\sigma_{I\ 1/2}}{d\omega} + \frac{d\sigma_{I\ 3/2}}{d\omega}\right] + (0.2)\ \frac{d\sigma_{II\ 1/2}}{d\omega} \quad . \tag{10}$$

The approximation $\frac{d\sigma_{I\ 3/2}}{d\omega} \simeq \frac{d\sigma_{II\ 1/2}}{d\omega}$ is made; this is suggested by theoretical evidence[27] that, with respect to each asymptote, $V_{II\ 1/2} \simeq V_{I\ 3/2}$ over the range of internuclear distances probed, and by the identical velocities of the $^2P_{1/2}$ and $^2P_{3/2}$ halogen atoms. The calculated $d\sigma_{el}/d\omega$ are transformed to the laboratory frame with velocity and angular averaging representative of the experimental configuration. By varying the $V_{I\ 1/2}$ and $V_{I\ 3/2}$ potentials to achieve a best fit to the experimental $I(\Theta)$, $V_{I\ 1/2}$ and $V_{I\ 3/2}$ are determined.

B. Interaction Potentials

The basis of the computations is the experimentally derived[10-12] $V_{I\ 1/2}$ and $V_{I\ 3/2}$, which are the BO potential curves, that is, the eigenvalues of the total electronic Hamiltonian over the range of R. Following Refs. 16(a,d) and 17, the total Hamiltonian is written as a sum of the electrostatic and spin orbit interactions: $H_{tot} = H_{el} + H_{so}$. H_{so} is assumed R independent. The matrix elements

$$\langle R, j, \Omega | H_{tot} | R j' \Omega' \rangle \equiv H^{\Omega}_{jj}, \tag{11}$$

are diagonal in Ω, and given by

$$H^{3/2}_{3/2,3/2} = V_{\Pi} - \Delta \tag{12a}$$

$$H^{1/2}_{1/2,1/2} = 1/3\ V_\Sigma + 2/3\ V_\Pi \quad , \tag{12b}$$

$$H^{1/2}_{3/2,3/2} = 2/3\ V_\Sigma + 1/3\ V_\Pi - \Delta \tag{12c}$$

$$H^{1/2}_{1/2,3/2} = H^{1/2}_{3/2,1/2} = \frac{\sqrt{2}}{3}\ (V_\Sigma - V_\Pi) \quad , \tag{12d}$$

where the V_Σ and V_Π are eigenvalues of H_{el}. The $\underset{\sim}{H}$ consists of 1 x 1 and 2 x 2 blocks with eigenvalues,

$$W(I\ 3/2) = V_\Pi - \Delta \tag{13a}$$

$$W(I\ 1/2) = 1/2[V_\Sigma + V_\Pi - \Delta - D] \tag{13b}$$

$$W(II\ 1/2) = 1/2[V_\Sigma + V_\Pi - \Delta + D] \tag{13c}$$

where

$$D = [(V_\Sigma - V_\Pi)^2 + \Delta^2 - 2/3\ \Delta\ (V_\Sigma - V_\Pi)]^{1/2} \quad . \tag{13d}$$

Thus, from the determined $V_{I\ 3/2}$, one obtains V_Π directly and V_Σ algebraically; the latter is given by

$$V_\Sigma = [2/3\ \Delta\ V_\Pi + V_\Pi\ W(I\ 1/2) - \Delta W(I\ 1/2) - \{W(I\ 1/2)\}^2]/[V_\Pi - W(I\ 1/2) - 1/3\ \Delta] \quad . \tag{14}$$

W(II 1/2) can be found from Eq. (13c).

To further specify the potential symbols used in relation to the $^2P_{1/2} + {}^1S_0$ energy zero, one notes

$$W(I\ 3/2) = V_\Pi - \Delta = V_{I\ 3/2} - \Delta \quad , \tag{15a}$$

$$W(I\ 1/2) = V_{I\ 1/2} - \Delta \quad , \tag{15b}$$

$$W(II\ 1/2) = V_{II\ 1/2} \quad , \tag{15c}$$

and in the limit of large R,

$$V_{\Pi} = V_{\Sigma} = V_{I\ 1/2} = V_{I\ 3/2} = V_{II\ 1/2} = W(II\ 1/2) = 0 \quad . \tag{15d}$$

In Reid's approach[18] the molecular electrostatic potential is expanded in Legendre polynomials, dependent on the angle formed by the direction of the unpaired p orbital $\vec{r}$ with respect to the internuclear position $\vec{R}$,

$$V(r,R) = \sum_i V_i(r,R)\ P_i(\vec{r}\cdot\vec{R}) \quad . \tag{16}$$

Only two terms contribute to the expansion giving

$$V_{\Sigma} = V_0 + 2/5\ V_2 \ ;\ V_{\Pi} = V_0 - 1/5\ V_2 \quad , \tag{17a}$$

or

$$V_0 = (V_{\Sigma} + 2\ V_{\Pi})/3 \ ;\ V_2 = 5/3(V_{\Sigma} - V_{\Pi}) \quad . \tag{17b}$$

Substituting V_0 and V_2 into Eq. (13) gives

$$W(I\ 3/2) = V_0 - 1/5\ V_2 - \Delta \tag{18a}$$

$$W(I\ 1/2) = (V_0 + 1/10\ V_2 - \Delta/2) - D' \tag{18b}$$

$$W(II\ 1/2) = (V_0 + 1/10\ V_2 - \Delta/2) + D' \tag{18c}$$

where

$$D' = 1/2[25\Delta^2 - 10\,\Delta\,V_2 + 9\,V_2^2]^{1/2} \quad . \tag{18d}$$

Alternatively, one has

$$V_0 = 1/3\ [W(I\ 1/2) + W(II\ 1/2) + W(I\ 3/2) + 2\Delta] \tag{19a}$$

$$V_2 = 5/3\ [W(I\ 1/2) + W(II\ 1/2) - 2W(I\ 3/2) - \Delta] \quad . \tag{19b}$$

Results

A. Numerical Considerations

The convergence of the $\underset{\sim}{S}$ was checked by varying the integration step size and end point. A step size of 1/(10k) (where k is the larger of the two values for the scattering channels) was used for the majority of computations. The integration starting point was kept at the origin and the end point fixed at 21 Å (however, see Results-D).

Some computations focused on the fine structure transition, and for these the computations were carried out to a J determined as the value that gave convergence of the inelastic channels ($\underset{\sim}{S}$ elements the size of 10^{-7}). For elastic scattering computations the maximum J was much larger and determined by the running sum of the elastic integral cross section not changing by more than ~1 part in 10^5 per J.

Integral cross sections calculated by different methods served as a consistency check in the present study. Agreement well within 1% was always found between $\sigma(j \rightarrow j')$ computed by direct summation (Eq. (5)), by numerical integration of the $d\sigma(j\rightarrow j')/d\omega$ (see Eqs. (3) and (4)),

$$\sigma = 2\pi \int_0^{\pi} \frac{d\sigma}{d\omega} \sin\theta d\theta \quad , \tag{20}$$

and by summation of the $\sigma(jmj \rightarrow j'mj')$ (see Eqs. (6)-(8)). In addition, for $^2P_{3/2} + {}^1S_0$ scattering, the elastic approximation gave integral cross sections typically within 1% of the CC results. The elastic σ_{el} were computed from

$$\sigma_{el}(j = 3/2 \rightarrow 3/2) = 1/2(\sigma_{I\ 1/2} + \sigma_{I\ 3/2}) \tag{21}$$

where $\sigma_{I\Omega} \equiv \sigma$ for $\Omega = 1/2$, $3/2$ is given by

$$\sigma = \frac{4\pi}{k^2} \sum_{\ell} (2\ell + 1) \sin^2\eta_\ell \quad , \tag{22}$$

with phase shifts corresponding to the use of $V_{I\ 1/2}$ or $V_{I\ 3/2}$ and calculated by the Numerov or JWKB methods.

Due to very rapid diffractive oscillations for these systems of large reduced masses μ, at the higher energies studied the angular spacing for the scattering amplitude, Eq. (4), used in CC calculation of $d\sigma/d\omega$ had to be reduced to 1/8° for $0° \leq \Theta \leq 90°$ in order to obtain smooth representations of $d\sigma/d\omega$, and accurate σ by Eq. (20). At larger angles for the higher energies, and over the complete angular range for the lower energies, a 1/2° spacing was satisfactory.

Comparisons of the $d\sigma/d\omega$ derived by the CC and elastic methods were carried out at energies chosen to coincide with nominal laboratory collision energies. At the temperature of the halogen atom beam sources, Boltzmann statistics predicts, for both F and Cl (coincidently), ~22% $^2P_{1/2}$ component. The supersonic expansion yields both spin orbit states at the same velocity (same collision energy). So, in order to include the $^2P_{1/2}$ scattering, the CC computations were performed at two energies for any given elastic comparison. For example, to compare the F + Ar CC and elastically derived $I(\Theta)$ for a laboratory relative collision energy E_{rel} of 0.108 eV, the CC equations were solved for E = 0.108 eV and 0.058 eV. From the first set of $\underset{\sim}{S}^J$, $d\sigma(1/2 \rightarrow 1/2,3/2)/d\omega$

were obtained, while the second set of $\underset{\sim}{S}^J$, $d\sigma(3/2 \rightarrow 1/2,\ 3/2)/d\omega$ could be obtained. Actually, $d\sigma(3/2 \rightarrow 1/2)/d\omega$ was conveniently obtained by detailed balance

$$(2j + 1)\ k_j^2 \frac{d\sigma(j \rightarrow j';k_j)}{d\omega} = (2j' + 1)\ k_{j'}^2 \frac{d\sigma(j' \rightarrow j;k_{j'})}{d\omega} \qquad (23)$$

The contribution of the four cross sections to the total scattering was weighted according to j (0.78 for j = 3/2 and 0.22 for j = 1/2), and center-of-mass (CM) to laboratory transformations were performed for the elastic and two inelastic transitions to arrive at the CC derived $I(\Theta)$. However, it is noted that $\sigma(j \rightarrow j')$ for $j \neq j'$ has a negligible contribution to $I(\Theta)$.

Representative cases for comparison of the CC and elastically calculated $I(\Theta)$ were taken to be: F + Xe at E_{rel} of 0.0915 and 0.456 eV; F + Ar at 0.0859, 0.108, and 0.481 eV; and Cl-Xe at 0.112 eV.

Two groups of CC computations for these systems were carried out. The first group of computations suffered from an error in V_0, V_2 (or V_Σ, V_Π) because the equivalency $V_{II\ 1/2} = V_{I\ 1/2}$ was made (the proper treatment is described in Theory-B). Analysis showed this error affected the two $\Omega = 1/2$ potentials, deepening the II 1/2 potential well and making the I 1/2 well more shallow. The net effect, in the classically accessible region, was to alter the $\Omega = 1/2$ potentials by ~10%, with the exception of the F-Ar, Xe II 1/2 states which were altered by ~20% (a small absolute change).

These runs could be used to test the sensitivity of the dynamics to the molecular potentials.

It was found that the sensitivity to the assumed equivalency of potentials was greatest for Cl-Xe, the case in which the $V_{I\ 3/2}$ is deepest; the second, proper set of computations showed an increase in the small $\sigma(1/2 \rightarrow 3/2)$ by nearly 80% for E = 0.00282 eV. The F-Ar, Xe systems showed a decrease in $\sigma(1/2 \rightarrow 3/2)$ of 40% at low energies and a decrease of ~20% at the highest energies, with the exception of a slight increase of $\sigma(1/2 \rightarrow 3/2)$ at the lowest energy (E = 0.0359 eV) for F-Ar. Thus $\sigma(1/2 \rightarrow 3/2)$ for these systems shows considerable sensitivity to the potentials.

For $d\sigma(3/2 \rightarrow 3/2)/d\omega$, only minor differences were found between the two groups of computations in the positions and shapes of the rainbow or orbiting oscillations. When the second group of computations was carried out correctly, it was found that $d\sigma(1/2 \rightarrow 1/2)/d\omega$ changed negligibly (for F-Ar,Xe), reflecting the small error in $V_{II\ 1/2}$ introduced in the first runs. The calculations were performed for values of E appropriate for the experimental E_{rel} of the $^2P_{3/2}$ level ($E_{rel} = E + \Delta$). Because of this agreement for the rather structureless $d\sigma(1/2 \rightarrow 1/2)/d\omega$, the fact that only a 22% contribution to the $I(\Theta)$ is involved, and the expense and effort involved in the CC computations, it was decided to forego repeating the computations for $E = E_{rel}$ for $^2P_{1/2}$ scattering with the exception of 0.108 eV for F-Ar displayed below. These $d\sigma(1/2 \rightarrow 1/2,3/2)/d\omega$ from the first group of computations are used only in the CC derived $I(\Theta)$ plots and only with small weighting, and in no way affect any conclusions.

Aside from the energies of the experimental comparison, CC computations at other energies were carried out for F-Ar and F-Xe to get a clearer trend for $\sigma(1/2 \rightarrow 3/2)$.

B. F-Xe

The potentials employed are shown in Fig. 1. Examples of some CC derived $d\sigma/d\omega$ are shown in Fig. 2 for the two elastic channels and a fine structure transition in the CM frame. Rainbow structure is clearly seen for $d\sigma(3/2 \rightarrow 3/2)/d\omega$. The $d\sigma(1/2 \rightarrow 1/2)/d\omega$ reflects the essentially repulsive II 1/2 state. The fast diffractive oscillations are seen to occur over the same angular range for both angular distributions $d\sigma(3/2 \rightarrow 1/2,3/2)/d\omega$; semiclassically, this indicates interference between different branches of the deflection function or quantum mechanically, multiple wavepacket interference. Another oscillatory structure is found in $d\sigma(3/2 \rightarrow 3/2)/d\omega$ that is in phase with the $d\sigma(3/2 \rightarrow 1/2)/d\omega$; these are undulations in the envelope of diffractive oscillations, which have only a small effect on the angular averaged results. Such oscillations are not found in the single channel calculations. The changing period of the oscillations in the fine structure transition $d\sigma/d\omega$ can be analyzed semiclassically[9] and indicates that for nearly head on collisions (large Θ) the difference in interfering impact parameters is smaller than at larger impact parameters (small Θ). The size of the $d\sigma(1/2 \rightarrow 3/2)/d\omega$ is nearly constant for all Θ. At lower energy, $d\sigma(3/2 \rightarrow 1/2)/d\omega$ shows broad undulations and lowered intensity.

The calculated $d\sigma/d\omega$ were converted to the laboratory frame and

the results are shown in Fig. 3 for E_{rel} = 0.456 eV in arbitrary units. The CC and elastic calculated I(Θ) are shown with and without angular averaging, and are displaced arbitrarily for clarity. All I(Θ) presented in this work correspond to a single collision energy (one Newton diagram). In the experimental analysis (Ref. 10-12) many Newton diagrams contribute to the velocity averaging, and such comparisons with experimental data can be found in these references. Figure 4 shows an angularly averaged I(Θ) comparison for E_{rel} = 0.0915 eV in which orbiting is present. Agreement between the CC and elastic I(Θ) for both these collision energies is extremely good. Values of CC computed $\sigma(j \rightarrow j)$ are listed in Table I.

Integral cross sections for fine structure transitions in F-Xe have been computed previously by both semiclassical[16d] and quantum mechanical[28] methods; however, they use quite different sets of potentials and large differences are found between the $\sigma(1/2 \rightarrow 3/2)$ reported in Refs. 16d, 28, and the present study. Table II lists $\sigma(1/2 \rightarrow 3/2)$ for a range of collision energies. The $\sigma(1/2 \rightarrow 3/2)$ rise steeply at low collision energies to a less rapid increasing rate at higher energies.

The $\sigma(jm_j \rightarrow j'm_j')$ can be evaluated from the B(j,j';g) by Eq. (7). The squares of the Clebsch-Gordan coefficients in Eq. (7) have been tabulated elsewhere[29] for these quantum numbers. Table III presents the calculated B(j,j';g). Note that B(3/2,3/2;g≠0), which corresponds to j = 3/2 intramultiplet ($m_j \neq m_{j'}$) transitions decrease slightly at higher E. This suggests that the effectiveness of the coupling responsible for these transitions is weakly proportional to the collision time.

B(j,j;g) for odd g are forbidden as first order processes[30] and show interstate coupling. It is therefore worthwhile to examine these more closely, as well as the B(1/2, 3/2;g), to gain further insight on the dynamics of these transitions. Note that $B(1/2,1/2;1) \equiv \sigma(1/2,1/2 \to 1/2,-1/2)$, $B(1/2,3/2;2) \equiv \sigma(1/2,1/2 \to 1/2,-3/2)$, and $B(3/2, 3/2;3) \equiv \sigma(3/2,3/2 \to 3/2,-3/2)$.

With this in mind, B_ℓ was computed for each step of the ℓ summation in Eq. (8). Results for $B_\ell(1/2,1/2;1)$, $B_\ell(1/2,3/2;1)$, $B_\ell(1/2,3/2;2)$, and $B_\ell(3/2,3/2;3)$ are shown in Fig. 5 for a total E = 0.0414 eV, and in Fig. 6 for E - 0.405 eV; the maximum ℓ values computed were 340 and 650, respectively.

At both energies the $B_\ell(1/2,3/2;g)$ show an oscillatory interference behavior with slightly different frequency components for g = 1,2. Significant contributions to B(1/2,3/2;2) extend to smaller ℓ. Note that $B_\ell(1/2,1/2;1)$ and $B_\ell(1/2,3/2;g)$ occur over the same region of ℓ but $B_\ell(1/2,1/2;1)$ shows a smooth structure overall, with a small oscillatory component superimposed for 0.405 eV with a slightly different frequency than $B_\ell(1/2,3/2;g)$. The $1/2,1/2 \to 1/2,-1/2$ transition at 0.405 eV shows stronger coupling to the 3/2 manifold, suggesting a model where part of the incoming j = 1/2 plane wave splits off and follows a lower adiabatic potential before rejoining the $^2P_{1/2}$ manifold. The decay of these transitions at high ℓ values (≃73 for 0.0414 eV and ≃200 for 0.405 eV) characterizes the extent of the classically sampled region of coupling, and so demarks the assumed localized coupling by the turning point for each of these ℓ. (If the

coupling is not localized, these turning points will delimit the large R range of coupling.) Approximating the $V_{II\ 1/2}$ by its ε and r_m (found from Eq. (13c)) and the remaining analytic potential parameters of $V_{I\ 3/2}$, the scattering analysis at 0.0414 and 0.405 eV give classical turning points of 3.5-3.7 Å characteristic of the nonadiabatic coupling inducing the intermultiplet transitions.

Also shown in Figs. 5 and 6 are the $B_\ell(3/2,3/2;3)$. They are seen to increase at large ℓ and the large ℓ values where they decay (~105,208) yield a coupling limit of 3.4-3.7 Å by turning point analysis for both $V_{I\ 1/2}$ and $V_{I\ 3/2}$ at both 0.0915 and 0.456 eV. Note that while the B(3/2,3/2;3) mildly decreases with increasing energy, the individual partial wave contributions to these B (B_ℓ) rather strongly decrease with increasing energy. Not shown are the oscillatory $B_\ell(3/2,3/2;1)$ which have the same large ℓ dependence as $B_\ell(3/2,3/2;3)$ but extend to somewhat smaller ℓ, and the oscillatory ℓ-wave contributions to B(3/2,3/2;2) which are quite broad and extend to smaller and larger ℓ. The $B_\ell(1/2,1/2;0)$ and $B_\ell(3/2,3/2;0)$ have the largest range. They are oscillatory in the region of ℓ's sampling the nonadiabatic coupling, and have a long smooth tail at large ℓ.

A final remark is made for [illegible]. In general the fine structure inelastic transitions can occur for $\ell' = \ell$ or $\ell \pm 2$. The $|\underset{\sim}{S}|^2$ were summed independently for these two channels, and a strong propensity for $\ell' = \ell \pm 2$ was found. The relative contributions to $\sigma(1/2 \to 3/2)$ for $\ell' = \ell \pm 2:\ell$ vary from 2.9:1 at 0.02 eV to 2.3:1 at 1 eV in a smooth fashion.

C. F-Ar

The potentials employed are shown in Fig. 7. Angular averaged CC and elastically derived I(Θ) are compared in Fig. 8 for E_{rel} = 0.108 eV and are in good accord. Similar agreement was obtained at 0.0859 eV and 0.481 eV. Note the low amplitude oscillations present in the I(Θ) derived from the CC dσ/dω at wide angles; these are comparable to oscillations found in the data (see Discussion).

We list selected CC computed integral elastic cross sections in Table IV, and values of σ(1/2 → 3/2) in Table V. The σ(1/2 → 3/2) of F-Ar are smaller than those for F-Xe but show a similar energy dependence; the weaker attractive interaction for F-Ar is perhaps indicative of weaker nonadiabatic coupling.

The B coefficients are presented for various E_{rel} in Table VI. The overall trends are similar to F-Xe. Plots of $B_\ell(1/2,1/2;1)$, $B_\ell(1/2,3/2;1)$, $B_\ell(1/2,3/2;2)$ and $B_\ell(3/2,3/2;3)$ versus ℓ for E = 0.0582 eV (maximum ℓ = 300) are shown in Fig. 9. The trends of these quantities versus ℓ at higher energies are qualitatively the same as F-Xe. Remarks about those B_ℓ coefficients not shown for F-Xe ($B_\ell(3/2,3/2;0,1,2)$ and $B_\ell(1/2,1/2;0)$) also apply here. Applying the turning point analysis used for F-Xe to the high ℓ damping of B_ℓ gives a strong coupling region in the vicinity of 3.1 Å (ℓ ≃ 60) for the intermultiplet and $^2P_{1/2}$ intramultiplet transitions and 3.1-3.2 Å (ℓ ≃ 84) for the $^2P_{3/2}$ intramultiplet transitions, again giving a common value for the region of nonadiabatic coupling between the $^2P_{1/2}$ and $^2P_{3/2}$ manifolds.

EPR linewidth measurements[31c] have been performed on F-Ar. From a semiclassical straight line trajectory model[31a,b] intramultiplet

cross sections were obtained from the linewidths. Plots of the B_ℓ coefficients show the model inadequately represents the CC computed transitions; deficiencies of the model have been noted previously.[31d,e] For the $^2P_{3/2}$ manifold no CC computations were carried out to permit direct comparison with the EPR study at 300°K; however, Table VI shows the slow variation of B(3/2,3/2;1,2,3) with energy. The listed values 0.0359 and 0.0582 eV. for the $^2P_{1/2}$ case are in the energy range for comparison with this gas cell experiment. The comparisons with the EPR derived cross sections are poor. The extrapolated CC values for the transitions $^2P_{3/2}|mj| = |3/2| \rightleftharpoons |1/2|$ are about a factor of two larger than given by Ref. 31c, while the CC values for the $^2P_{3/2}|mj| = 1/2 \rightleftharpoons -1/2$ cross sections are about a factor of three smaller, and the CC values for the $^2P_{1/2}|mj| = 1/2 \rightleftharpoons -1/2$ cross sections are about a factor of ten smaller. Considering the inadequacy of the model, we conclude that the cross sections of Ref. 31c do not provide a good test of the present calculations.

Four further tests to probe the sensitivity of the scattering cross sections to the V(R) were carried out for F + Ar at 0.0359 and 0.0582 eV. The potentials $V_{I\ 3/2}$ or $V_{I\ 1/2}$ were altered by changing one or two of the key parameters (ε, r_m, and β) of the MMSV analytic potential form by ~20%. The main interest was to see if the wide angle $d\sigma/d\omega$ oscillations could be amplified. (One other test equated the two C_6 constants--this had virtually no effect on any of the cross sections.) It was found that the oscillations could not be amplified, though they could be damped. One interesting case was found when the

$V_{I\ 1/2}$ β_1 parameter was increased from 4.3 to 5.3. This increased the $\sigma(1/2 \rightarrow 3/2)$ by a little more than a factor of two, with a slight decrease in $\sigma(1/2,1/2 \rightarrow 1/2,-1/2)$, and the wide angle oscillations were damped. The other potential variations had comparatively minor effect.

Finally, the propensity for $\ell' = \ell \pm 2:\ell$ for the $\sigma(1/2 \rightarrow 3/2)$ was found by the channel ratios 2.9:1 at 0.0359 eV to 2.2:1 at 0.431 eV, changing in a smooth fashion.

D. Cl-Xe

The potentials employed for this systems are shown in Fig. 10. The CC computations were carried out using tentative fits to the data; subsequently, improved fits to the data were found, and the recommended Cl-Xe $V_{I\ 1/2}$ and $V_{I\ 3/2}$ are contained in Ref. 12. However, the V(R) used here are close to the final values and the scattering cross sections should not differ markedly. The V(R) used here will provide a good test of the elastic approximation for I(Θ). For reference the MMSV parameters used here are given (analytic form is listed in Ref. 10): for the $V_{I\ 1/2}$, $\varepsilon = 0.0304$ eV, $r_m = 3.18$ Å, $\beta_1 = 5.5$, $\beta_2 = 3.6$, $X_1 = 1.237$, $X_2 = 1.750$, $C_6 = 80.7$ eV·Å^6, and $C_8 = 0$ eV·Å^8; for the $V_{I\ 3/2}$, $\varepsilon = 0.0147$ eV, $r_m = 4.10$ Å. $\beta_1 = 7.6$, $\beta_2 = 6.6$, $X_1 = 1.105$, $X_2 = 1.500$, $C_6 = 85.0$ eV·Å^6, and $C_8 = 620$ eV·Å^8.

To assure convergence of the elastic channels for this system a maximum J of 548.5 was used, which together with very low E = 0.00282 eV necessitated moving the final integration point, conservatively, to 100 Å.

A comparison of I(Θ) computed by CC and elastic methods for E_{rel} = 0.112 eV is shown in Fig. 11. Agreement is good, though not quite as

close as for the F systems. The much more attractive Cl-Xe van der Waals $V_{I\ 3/2}$ (V_{Π}) is likely responsible for the slightly poorer agreement. Note some perturbation of the CC diffractive oscillations, and small oscillations in the wide angle $d\sigma/d\omega$ though the inelastic cross section is very small.

The $\sigma(1/2 \rightarrow 1/2)$ at $E_{rel} = 0.00282$ eV is 717.5 $\mathring{A}^2$, $\sigma(3/2 \rightarrow 3/2)$ *at 0.112 eV is 403.7* $\mathring{A}^2$, $\sigma(1/2 \rightarrow 3/2) = 7.78$ *E-5* $\mathring{A}^2$ *at 0.00282 eV*, and the ratio of the $\ell' = \ell \pm 2$ to $\ell' = \ell$ channels for $\sigma(1/2 \rightarrow 3/2)$ is 3.0. Though the total energy here is just above zero, in general the $\sigma(1/2 \rightarrow 3/2)$ are expected to be smaller than for F-Ar,Xe due to the larger spin orbit splitting Δ of Cl, but this study does not probe this trend. To get an idea of the size of the $^2P_{3/2}$ intramultiplet transitions, and for completeness, the B coefficients are listed in Table VII.

Concerning the $\sigma(1/2 \rightarrow 3/2)$, the collision energy is just above threshold for the $3/2 \rightarrow 1/2$ transition (the 1/2 channel is barely open) and this is well inside the orbiting regime for $V_{II\ 1/2}$. Consequently, cross sections pertaining to the j = 1/2 level should not be considered indicative of a large energy range, though j = 3/2 manifold intramultiplet transitions will be indicative of the thermal energy range.

Figure 12 presents selected B_ℓ as a function of ℓ. The B_ℓ relating to j = 1/2 are small in magnitude and show resonances probably associated with the close approach of the centrifugal barrier to E. Penetration through the centrifugal barrier to quasibound levels will

give rise to the observed structure. This seems to be the case as a turning point analysis for the $V_{II\ 1/2}$ at 0.00282 eV (again in the fashion employed for F-Xe) showed that for $\ell = 48$ the centrifugal barrier reached E. The previous turning point (for $\ell = 47$) was 3.75 Å, while at a few higher ℓ values the turning point was ~7 Å. Thus the turning point analysis can only bracket the coupling region, and shows why the ℓ decay of the $B_\ell(1/2,j';g)$ is so sudden. The 0.112 eV analysis for the $V_{I\ 1/2}$ and $V_{I\ 3/2}$ give a common turning point of ~4.0 Å using $\ell \simeq 165$ for the $B_\ell(3/2,3/2;3)$.

Discussion

The close agreement between the I(Θ) computed by the CC and elastic methods shows that the simple single channel approach to these RG-X three channel scattering problems is useful for extracting realistic V(R) from experimental I(Θ). Use of realistic V(R) then makes the coupled-channels calculation meamingful for comparison or prediction of experimental quantities. It is difficult to assess how widely applicable this elastic method is to other electronic open shell systems when the spin orbit splitting is not as large as for the RG-X systems studied here. Certainly at hyperthermal energies where higher electronic states may become strongly coupled, the approximation is expected to deteriorate. We find poorer agreement between I(Θ) computed by elastic and CC methods for Cl-Xe than for the F-RG systems. The Br- and I-RG systems, likely to have comparable and non-negligible attractive $V_{I\ 1/2}$ and $V_{I\ 3/2}$, probably will have their scattering less well represented by Eq. (9a), but sufficiently approximated to allow valid I(Θ) analysis. Useful application to nonhalogen scattering with electronic states in qualitative resemblance to those here remains to be seen, as does that for strongly chemically bound systems. Of course, the more electronic states involved, the more smearing will appear in dσ/dω.

The elastic models (see Ref. 21 and references cited therein) previously used for small spin orbit coupling rest on the assumption that during the collision the electron orbital angular momentum and spin become uncoupled, and that coupling is weak between the adiabatic

states of the electrostatic electronic Hamiltonian. The physical meaning of the elastic analysis used here is that the electron orbital and spin angular momentum remain coupled throughout the collision, and coupling is weak between the adiabatic states of the total electronic Hamiltonian including spin orbit interaction.

An early motivation for this study was a desire to answer the question of the meaning of some small amplitude oscillations in the experimental $I(\theta)$; this is a small effect under scrutiny. The data are often ambiguous and possibly the random error analysis may not be giving reliable uncertainties, yet, at least for F-Ar, CC derived $I(\Theta)$ are in semiquantitative agreement with the data. Remaining disagreement could rest in the data itself, insufficiently accurate $V(R)$, or in the assumptions used in carrying out the CC computations. The latter include possible underestimation of coupling to electronic states a few eV distant, underestimates of the BO coupling terms, and neglect of nuclear spin, though these all seem unlikely. Perhaps a more probable error is the assumption that the spin orbit interaction is constant over the internuclear distances probed by the scattering, especially for the anomalous F-Xe system (see discussion in Ref. 11). More efforts directed toward calculating the molecular spin orbit interaction from first principles is needed.

Plots of slected $B_\ell(j,j';g)$ versus ℓ reveal information about the collision dynamics. The $B_\ell(1/2,1/2;1)$ have the same range of ℓ contribution as the $B_\ell(1/2,3/2;g)$ supporting a common mechanism. Yet the lack of oscillations found in the low energy $B_\ell(1/2,1/2;1)$ and the

appearance of a minor oscillatory component at higher energy have been a surprising contrast to the $B_\ell(1/2,3/2;g)$ oscillatory structure. This has prompted a suggestion that for $j = 1/2$ intramultiplet transitions at higher energies, in addition to the virtual transitions to the $^2P_{3/2}$ manifold, true double passage transitions out of and back to the $^2P_{1/2}$ manifold are occurring.

It is likely that nonadiabatic coupling in these systems is localized.[32] The local ℓ wave dependence of the critical B coefficients support this as follows. The classical turning point analysis employed for the large ℓ decay of $B_\ell(j,j;g)$ for odd g, and $B_\ell(1/2,3/2;g)$ has pointed to a common nonadiabatic coupling region for <u>both</u> inter- and intramultiplet transitions. This analysis is approximate, mostly due to the somewhat arbitrary choice of ℓ wave cut-off and approximate form of $V_{II\ 1/2}$, but the derived values probably are accurate as seen by the agreement of the turning points found for the adiabatic potentials at more than one energy for F-Ar,Xe, and the ability to explain the sharp ℓ cut-off for Cl-Xe. The critical turning points occur where the $V_{I\ 1/2}$ and $V_{I\ 3/2}$ splitting is still small. Undoubtedly the best explanation of this phenomena was given in 1932 by Stückelberg.[33] The nonadiabatic coupling is localized at where the adiabatic curves cross, and, here, this occurs in the complex plane for the $\Omega = 1/2$ adiabatic potentials, with the real R' component determined by

$$V_\Sigma - V_\Pi = -\Delta/3 \quad . \tag{24}$$

For the potential employed here, to the nearest 0.1 Å, for F-Xe R' = 3.6 Å, for F-Ar 3.0 Å, and for Cl-Xe 3.7 Å. The coincidence of

these values with those of the turning point analysis of the fully quantum mechanical results is not accidental (and employing the $V_{I\ 3/2}$ in the analysis is not warranted). The small $I(\Theta)$ oscillations observed in the laboratory and computed by the CC method should properly by termed Stückelberg oscillations.[34] It is also noteworthy that $d\sigma/d\omega$ perturbations appear for Cl-Xe even though Δ is much larger for Cl than for F, and the $\sigma(1/2 \rightarrow 3/2)$ is very small for the energy studied. Further study is needed to understand more fully the role of the complex V and R planes in molecular interactions.

Summary and Conclusions

Coupled-channel scattering calculations have been carried out in the thermal energy range using realistic interaction potentials for F-Xe, F-Ar, and Cl-Xe. These calculations support, by differential cross section comparisons, an elastic scattering model appropriate to Hund's case c, by which the V(R) have been derived. The CC derived $d\sigma/d\omega$ show perturbations due to nonadiabatic coupling, in qualitative or semiquantitative agreement with experimental[10-12] $I(\Theta)$. These are assumed to be Stückelberg oscillations based on the consistent agreement between classical turning points derived from the $B_\ell(j,j;g)$ for odd g, and $B_\ell(1/2,3/2;g)$ (intra- and intermultiplet transitions) decay as a function of nuclear orbital angular momentum and the real component of the complex crossing point between the $\Omega = 1/2$ adiabatic potentials. The strong positive energy dependence of $\sigma(1/2 \rightarrow 3/2)$ and $\sigma(1/2,1/2 \rightarrow 1/2,-1/2)$ indicate an ability to reach this complex crossing with enough momentum to pass through the crossing before adiabatic relaxation. On the other hand, the $^2P_{3/2}$ integral intramultiplet transitions show a weak negative energy dependence and a strong negative energy dependence for individual partial wave contributions even though they also are characterized by the same localized nonadiabatic crossing.

The question of the accuracy of approximating the molecular spin orbit coupling by the atomic value over a substantial range of internuclear distances is raised, especially for the Xe systems.

References

1. (a) H. S. W. Massey, Electronic and Ionic Impact Phenomena, Vol. III (Oxford, 1971); (b) J. B. Hasted, Physics of Atomic Collisions, 2nd ed (American Elsevier, New York, 1972), Chapter 13; (c) L. Krause, Adv. Chem. Phys., Vol. XXVIII (1975), Chapter 4; (d) E. E. Nikitin, ibid, Chapter 5.

2. B. Kamke, Z. Physik A273, 23 (1975).

3. L. K. Lam, A. Gallagher, and R. Drullinger, J. Chem. Phys. 68, 4411 (1978); A. Gallagher in Atomic Physics 4, ed. G. zu Putlitz, E. W. Weber, A. Winnacker (Plenum, New York, 1975).

4. R. E. Smalley, D. A. Auerbach, P. S. H. Fitch, D. H. Levy, and L. Wharton, J. Chem. Phys. 66, 3778 (1977).

5. R. Ahmad-Bitar, W. P. Lapatovich, D. E. Prichard, I. Renhorn, Phys. Rev. Lett. 39, 1657 (1977).

6. K. T. Gillen, R. P. Saxon, and D. C. Lorents, Phys. Rev. A 13, 2033 (1976).

7. R. E. Olson and F. T. Smith, Phys. Rev. A 3, 1607 (1971).

8. G. M. Carter, D. E. Pritchard, M. Kaplan, and T. W. Ducas, Phys. Rev. Lett. 35, 1144 (1975).

9. R. Düren and H.-O. Hoppe, J. Phys. B 11, 2143 (1978).

10. C. H. Becker, P. Casavecchia, and Y. T. Lee, J. Chem. Phys. 69, 2377 (1978) (Chapter I).

11. C. H. Becker, P. Casavecchia, and Y. T. Lee, J. Chem. Phys. (in press) (Chapter II).

12. C. H. Becker, J. J. Valentini, P. Casavecchia, S. J. Sibener, and Y. T. Lee, Chem. Phys. Lett. (in press) (Chapter III).

13. W. D. Phillips, C. L. Glaser, and D. Kleppner, Phys. Rev. Lett. 38, 1018 (1977); R. W. Anderson, T. P. Goddard, C. Porravand, and J. Warner, J. Chem. Phys. 64, 4037 (1976); J. Apt and D. E. Prichard, Phys. Rev. Lett. 37, 91 (1976).

14. J. Pascale, J. Chem. Phys. 69, 2788 (1978).

15. V. Aquilanti and P. Casavecchia, J. Chem. Phys. 64, 731 (1976); V. Aquilanti and P. Casavecchia, ibid. 65, 5518 (1976).

16. (a) E. E. Nikitin, J. Chem. Phys. 43, 744 (1965); (b) E. I. Dashevskaya, F. Masnou-Seews, R. McCarrol, and E. E. Nikitin, Opt. Spectrosc. 37, 119 (1974); (c) F. Masnou-Seews and R. McCarrol, J. Phys. B 7, 2230 (1974); (d) R. K. Preston, C. Sloane, and W. H. Miller, J. Chem. Phys. 60, 4961 (1974); (e) J. Pascale and P. M. Stone, J. Chem. Phys. 65, 5122 (1976); (f) E. L. Lewis and L. F. McNamara, Phys. Rev. A 5, 2643 (1972); (g) C. F. Melius and W. A. Goddard III, Phys. Rev. A 10, 1541 (1974).

17. F. H. Mies, Phys. Rev. A 7, 942 (1973); ibid., 7, 957 (1973).

18. (a) R. H. G. Reid and A. Dalgarno, Phys. Rev. Lett. 22, 1029 (1969); (b) R. H. G. Reid, J. Phys. B 6, 2018 (1973).

19. F. Rebenstrost and W. A. Lester, Jr., J. Chem. Phys. 67, 3367 (1977).

20. J. M. Launay, J. Phys. B 10, 3665 (1977).

21. R. H. G. Reid, J. Phys. B 8, L493 (1975); R. H. G. Reid and R. F. Franklin, ibid. 11, 55 (1978); C. Harel, V. Lopez, R. McCarroll, A. Riera, and P. Wahnon, ibid. 11, 71 (1978); B. Amaee and C. Bottcher, ibid. 11, 1249 (1978).

22. B. R. Johnson, J. Comp. Phys. 13, 445 (1973).

23. W. H. Miller, J. Chem. Phys. 50, 407 (1969); see also J. Schaefer and W. A. Lester, Jr., ibid. 62, 1913 (1975).

24. M. E. Rose, Elementary Theory of the Angular Momentum (Wiley, New York, 1957), pp. 48-73; D. M. Brink and G. R. Satchler, Angular Momentum, 2nd ed. (Oxford, 1968), pp. 13-37.

25. G. Grawert, Z. Physik 225, 283 (1969).

26. See, e.g., Ref. 1a, pp. 1870-1873, and R. P. Marchi and F. T. Smith, Phys. Rev. 139, A1025 (1965).

27. T. H. Dunning and P. J. Hay, J. Chem. Phys. 69, 134 (1978).

28. P. L. DeVries, M. S. Mahlab, and T. F. George, Phys. Rev. A 17, 546 (1978).

29. Ref. 18b, Table 2.

30. See, e.g., Refs. 17, 18b, and A. D. Wilson and Y. Shimoni, J. Phys. B 7, 1543 (1974).

31. (a) T. J. Cook and T. A. Miller, J. Chem. Phys. 59, 1342 (1973); (b) T. J. Cooke and T. A. Miller, ibid. 59, 1352 (1973); (c) B. R. Zegarski, T. J. Cook, and T. A. Miller, ibid. 62, 2952 (1975); (d) G.J. Fisanick-Englot and T. A. Miller, ibid. 64, 786 (1976); (e) G. J. Fisanick-Englot and T. A. Miller, ibid. 66, 1175 (1977).

32. See, e.g., Refs. 1d and 16d.

33. E. G. G. Stückelberg, Helv. Phys. Acta 5, 369 (1932); see also W. H. Miller and T. F. George, J. Chem. Phys. 56, 5637 (1972); Ref. 16(d); and Ref. 1(d), Sec. VA.

34. See. e.g., Ref. 16(d), and M. S. Child, Molecular Collision Theory, Academic Press, London (1974), Sec. 8.5.

Table I. Elastic Integral Cross Sections in $Å^2$ for F-Xe at Relative Collision Energies E_{rel}.

E_{rel}(eV)	j	$\sigma(j \rightarrow j)$
0.0414	1/2	311.1
0.405	1/2	207.2
0.0915	3/2	241.7
0.456	3/2	188.2

Table II. F-Xe Fine Structure Transition Integral Cross Sections

E (eV)	$\sigma(j = 1/2 \rightarrow 3/2)$ ($Å^2$)
0.020	0.00506
0.0414	0.0197
0.150	0.204
0.300	0.715
0.405	1.088
0.600	1.897
0.800	2.675
1.000	3.453

Table III. B(j,j';g) in $Å^2$ for F-Xe at Relative Collision Energies E_{rel}

E_{rel} (eV)	j → j'		g = 0	1	2	3
0.0141	1/2	1/2	6.22E+2	2.21E-2		
0.0414	1/2	3/2		3.62E-4	7.64E-3	
0.0915	3/2	3/2	8.15E+2	1.23E+1	2.09E+1	1.40E0
0.405	1/2	1/2	4.13E+2	3.40E-1		
0.405	1/2	3/2		9.57E-2	3.78E-1	
0.456	3/2	3/2	6.29E+2	1.13E+1	1.68E+1	8.88E-1

Table IV. Integral Elastic Cross Sections in $Å^2$ for F-Ar at Relative Collision Energies E_{rel}.

E_{rel} (eV)	j	σ(j → j)
0.108	1/2	175.4
0.431	1/2	130.2
0.108	3/2	165.9
0.456	3/2	130.7

Table V. F-Ar Fine Structure Changing Integral Cross Sections

E (eV)	$\sigma(1/2 \rightarrow 3/2)$ ($Å^2$)
0.0359	0.00122
0.0582	0.00529
0.108	0.0349
0.200	0.128
0.300	0.314
0.431	0.700

Table VI. B(j,j';g) in $Å^2$ for F-Ar at Relative Collision Energies E_{rel}

E_{rel} (eV)	j	j'	g = 0	1	2	3
0.0359	1/2	1/2	3.70E2	1.14E-2		
0.0359	1/2	3/2		3.87E-5	4.62E-4	
0.0859	3/2	3/2	5.82E2	5.82E0	1.57E1	9.67E-1
0.0582	1/2	1/2	3.17E2	2.22E-2		
0.0582	1/2	3/2		2.83E-4	1.94E-3	
0.108	3/2	3/2	5.65E2	5.89E0	1.47E1	9.37E-1
0.108	1/2	1/2	3.51E2	5.49E-2		
0.108	1/2	3/2		2.18E-3	1.26E-2	
0.158	3/2	3/2	5.50E2	6.14E0	1.42E1	9.06E-1
0.431	1/2	1/2	2.59E2	3.57E-1		
0.431	1/2	3/2		1.03E-1	2.18E-1	
0.481	3/2	3/2	4.34E2	7.24E0	1.20E1	8.87E-1

Table VII. B(j,j';g) in $Å^2$ for Cl-Xe at Relative Collision Energy E_{rel}

E_{rel} (eV)	j → j'		g = 0	1	2	3
0.00282	1/2	1/2	1.43E3	1.10E-3		
0.00282	1/2	3/2		4.20E-7	3.08E-5	
0.112	3/2	3/2	1.44E3	1.18E1	2.50E1	1.25E0

Figure Captions

Fig. 1. The F-Xe interaction potentials for the I 1/2, I 3/2, and II 1/2 states (——) are shown in eV vs Å. The Π and Σ potentials (- - -) governed solely by electrostatic forces, are also shown in eV. The derived V_0 and V_2 (——) are given in hartree vs Å. The energy zero is the $^2P_{1/2} + {}^1S_0$ asymptote.

Fig. 2. Absolute ($Å^2$) differential cross sections for F-Xe in the center-of-mass frame. (a) j = 1/2 → 1/2 at relative collision energy E_{rel} = 0.406 eV. This curve has been displaced upwards one order of magnitude for clarity. (b) j = 3/2 → 3/2 at E_{rel} = 0.456 eV. (c) $d\sigma(1/2 \to 3/2)/d\sigma$ at E_{rel} = 0.406 eV (= (0.455) $d\sigma(3/2 \to 1/2)/d\omega$ at E_{rel} = 0.456 eV).

Fig. 3. Comparison of F-Xe I(θ) derived by CC and elastic methods for E_{rel} = 0.456 eV. Arbitrary scaling is employed. (a) CC result with no angular averaging. (b) Elastic result with no angular averaging. (c) Angular average of curve (a). (d) Angular average of curve (b).

Fig. 4. Comparison of F-Xe I(θ) derived by CC and elastic methods for E_{rel} = 0.915 eV. (a) CC results angular averaged. Slight jagged quality is due to 1/2° spacing. (b) Elastic results angular averaged.

Fig. 5. Absolute ($Å^2$) (a) $B_\ell(1/2,1/2;1)$, (b) $B_\ell(1/2,3/2;1)$, (c) $B_\ell(1/2,3/2;2)$ and (d) $B_\ell(3/2,3/2;3)$ versus ℓ, the nuclear orbital angular momentum, for F-Xe at the total E = 0.0414 eV. Note individual scaling shown.

Fig. 6. Same as in Fig. 5, except for E = 0.405 eV, F-Xe.

Fig. 7. The F-Ar interaction potentials. Same notation as Fig. 1.

Fig. 8. Same as in Fig. 4, except for F-Ar at E_{rel} = 0.108 eV.

Fig. 9. Same as Fig. 5 except for F-Ar at E = 0.0582 eV.

Fig. 10. The Cl-Xe interaction potentials. Same notation as Fig. 1. Note these potentials are slightly different than the recommended values of Ref. 12, see text.

Fig. 11. Same as in Fig. 3, except for Cl-Xe at E_{rel} = 0.112 eV.

Fig. 12. Same as in Fig. 5, except for Cl-Xe at E = 0.00282 eV.

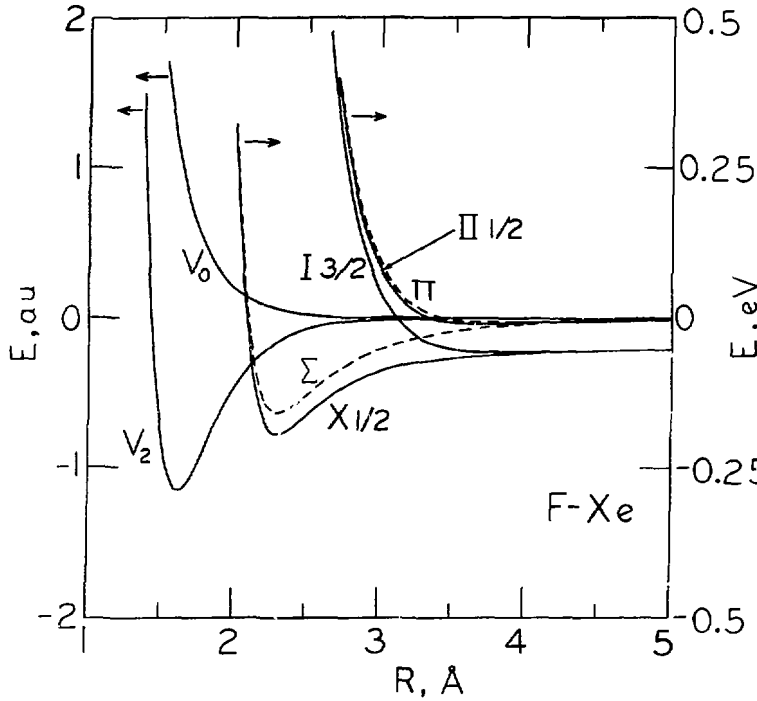

XBL 7811-12991

Fig. 1

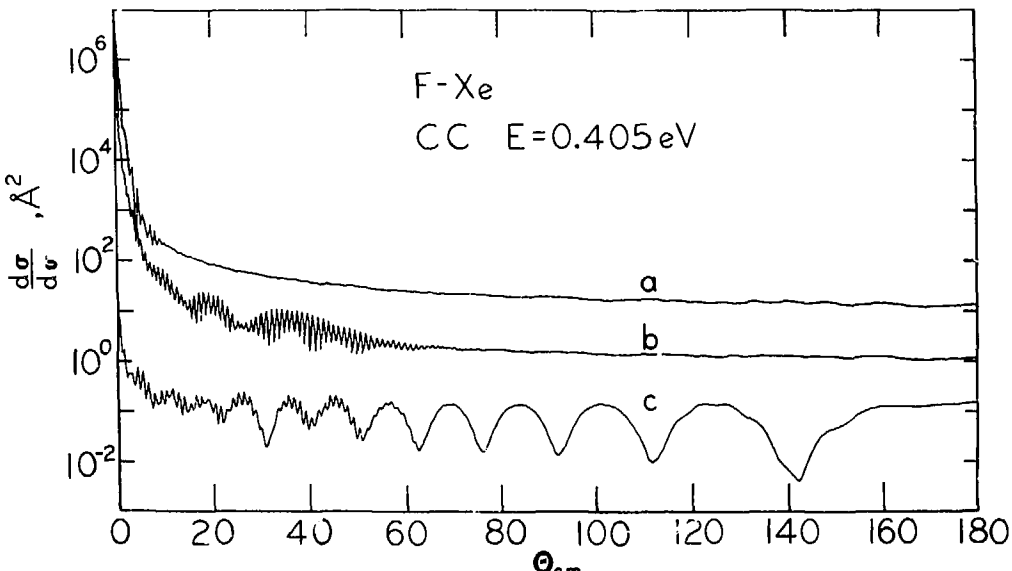

XBL 7811-12994

Fig. 2

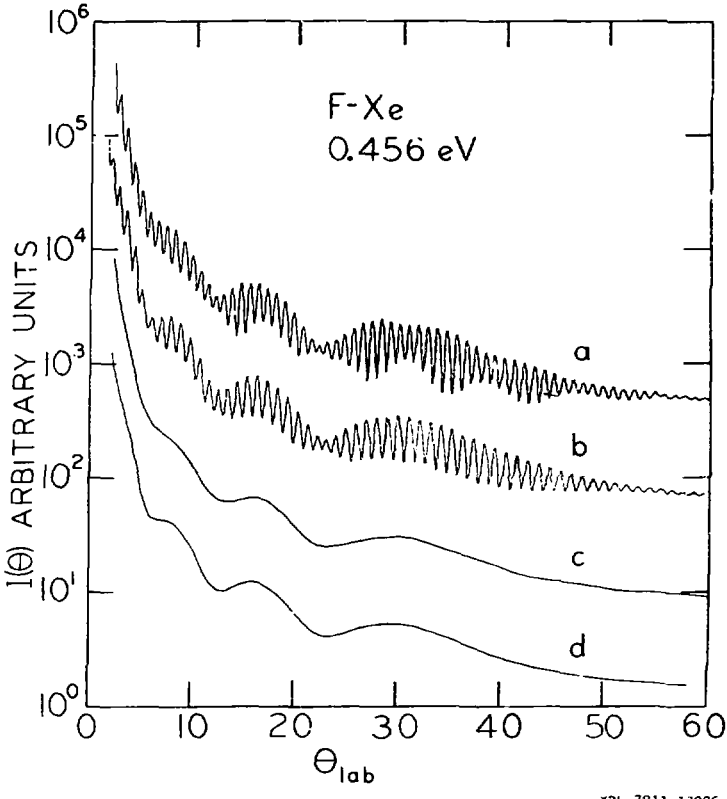

XBL 7811-12996

Fig. 3

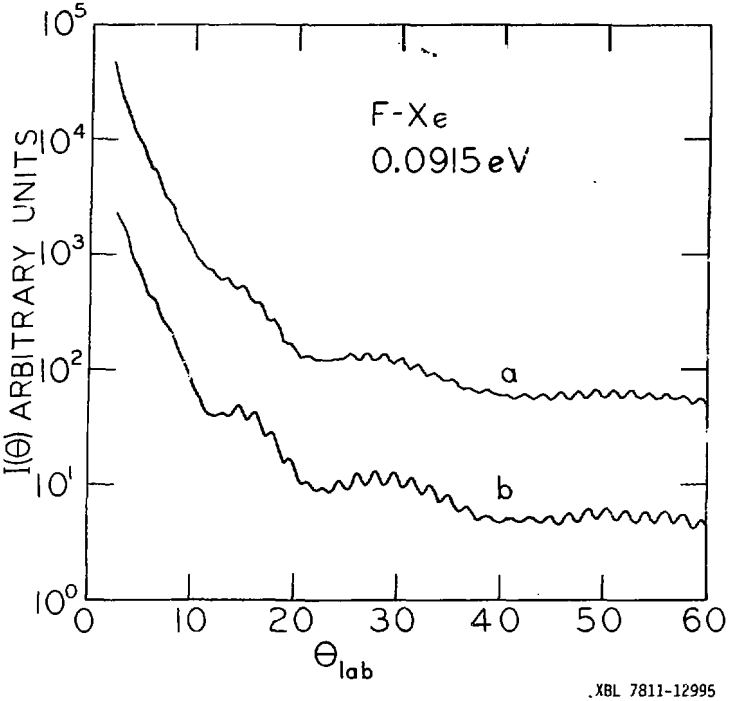

XBL 7811-12995

Fig. 4

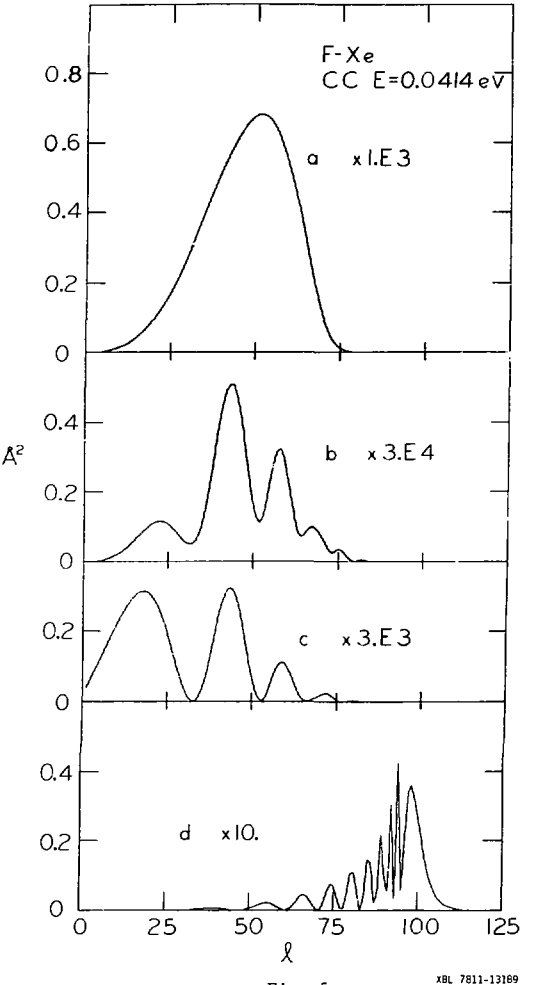

XBL 7811-13189

Fig. 5

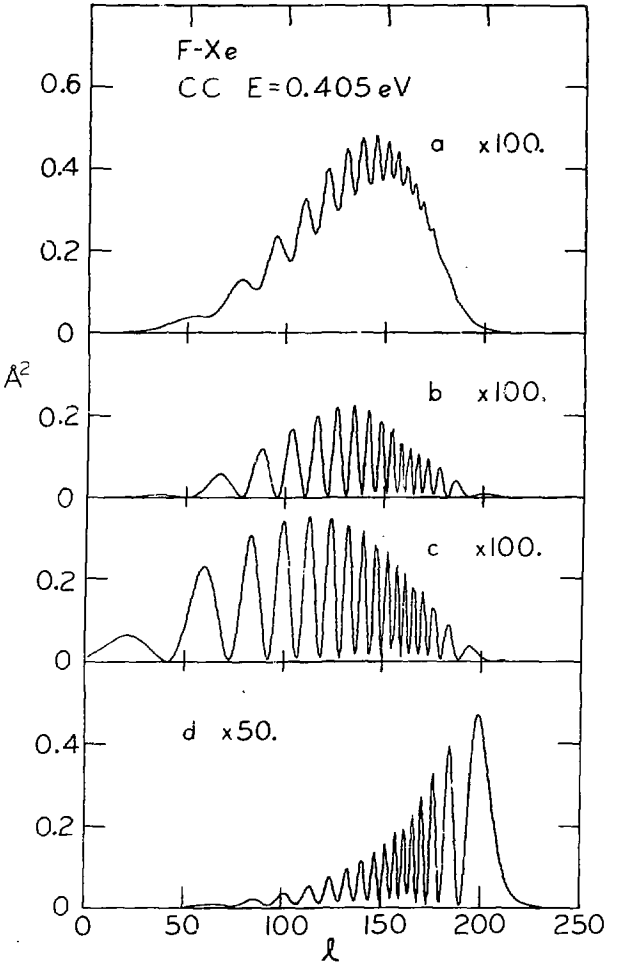

Fig. 6

XBL 7812-13190

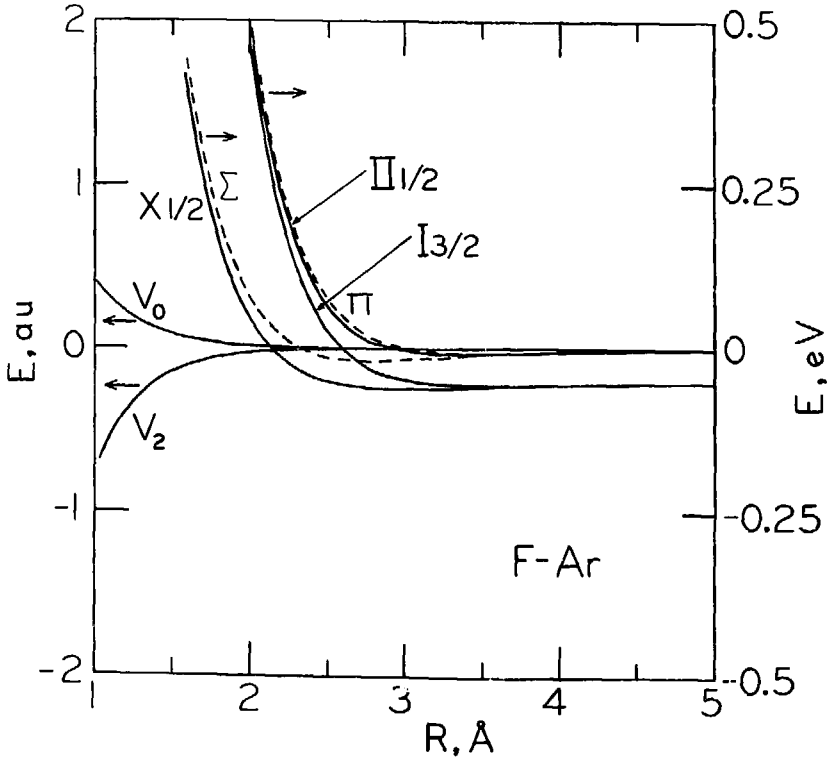

XBL 7811-12993

Fig. 7

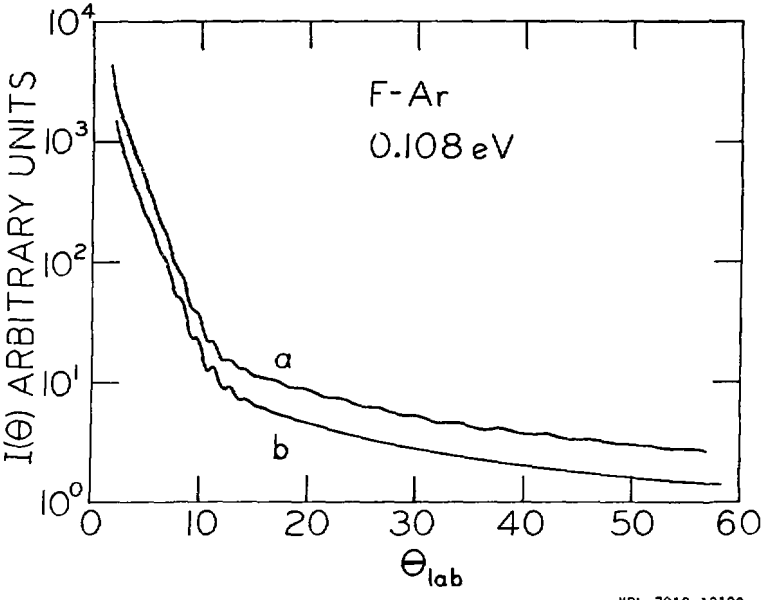

XBL 7812-13199

Fig. 8

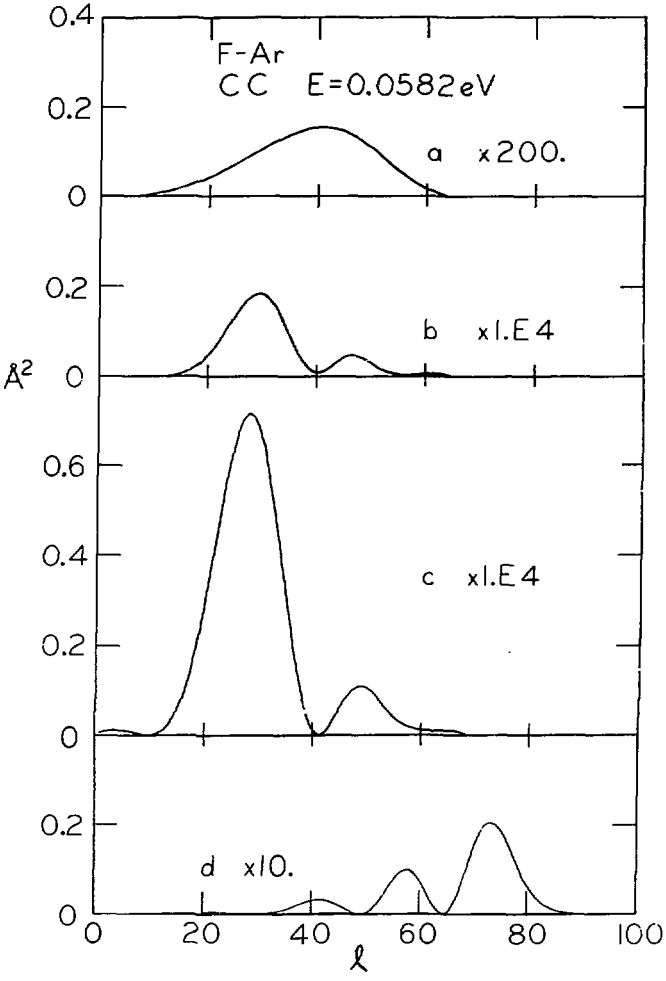

Fig. 9

XBL 7812-13201

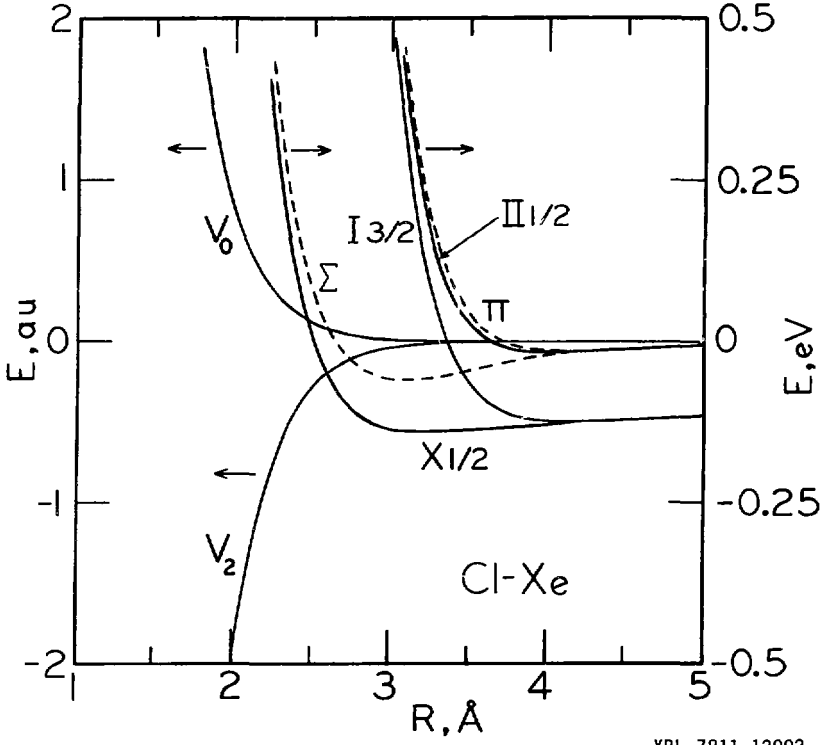

XBL 7811-12992

Fig. 10

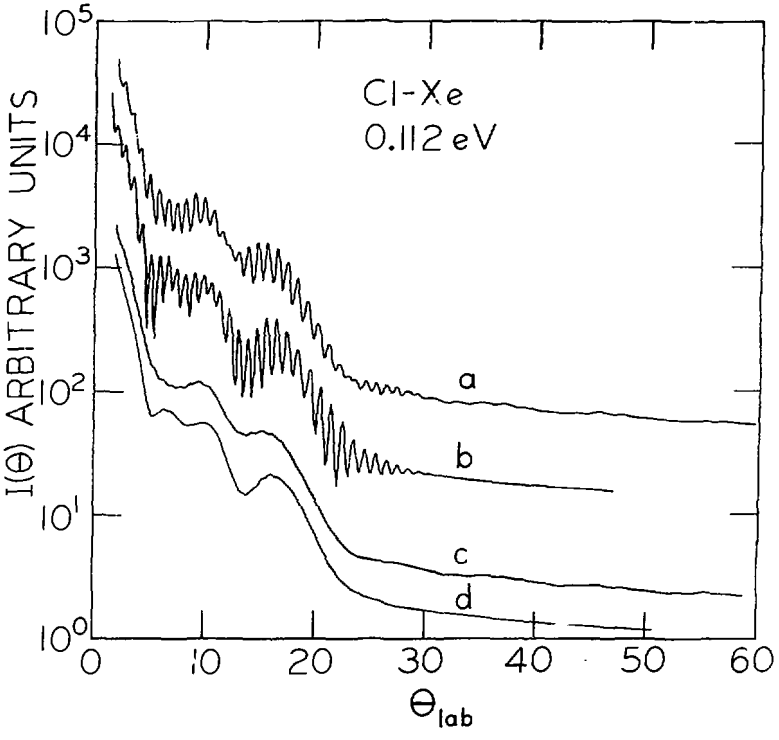

Fig. 11

XBL 7812-13200

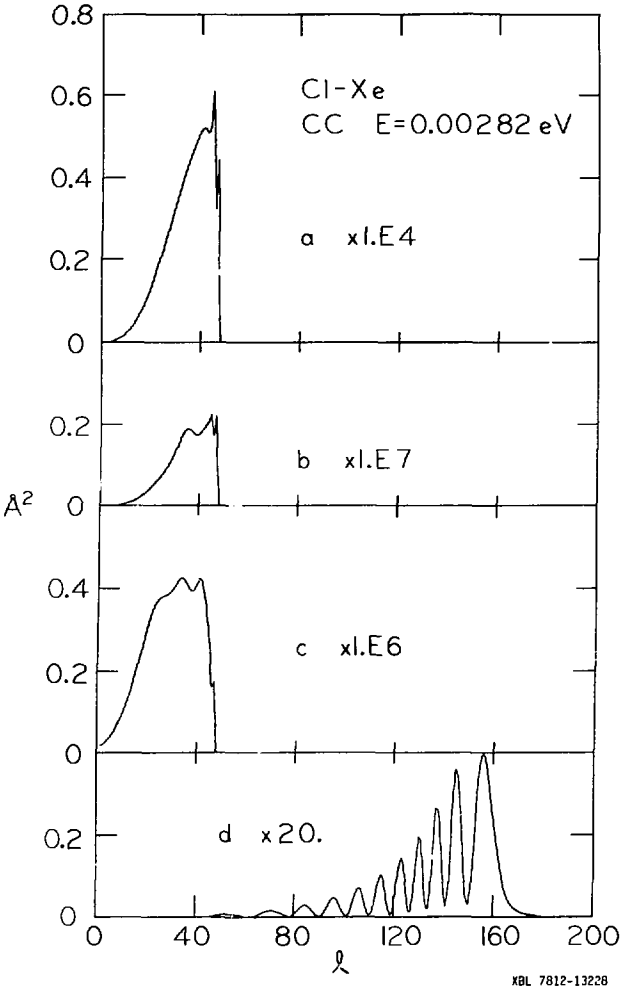
0.8
0.6
0.4
0.2
0
Cl-Xe
CC E=0.00282 eV
a x1.E4
0.2
0
b x1.E7
Å²
0.4
0.2
0
c x1.E6
0.2
0
d x20.
0
40
80
120
160
200
ℓ
XBL 7812-13228

Fig. 12